University of Alberta

Numerical Characterization of Ultrasound Elastography for the Early Detection of Deep Tissue Injuries

by

Kenton Hamaluik

A thesis submitted to the Faculty of Graduate Studies and Research in partial fulfilment of the requirements for the degree of

Master of Science

Department of Mechanical Engineering

Fall 2013
Edmonton, Alberta

Abstract

Deep tissue injuries are subcutaneous regions of extreme tissue breakdown generally induced by the application of significant mechanical pressure over extended periods of time through the biological mechanisms of ischemia and cell deformation causing rupture. These wounds are commonly suffered as a secondary wound or disease, often formed due to extended periods of motionless such as stationary sitting in spinal cord injured patients or those undergoing surgery.

Acknowledgements

Lorem ipsum dolor sit amet, consectetuer adipiscing elit. Ut purus elit, vestibulum ut, placerat ac, adipiscing vitae, felis. Curabitur dictum gravida mauris. Nam arcu libero, nonummy eget, consectetuer id, vulputate a, magna. Donec vehicula augue eu neque. Pellentesque habitant morbi tristique senectus et netus et malesuada fames ac turpis egestas. Mauris ut leo. Cras viverra metus rhoncus sem. Nulla et lectus vestibulum urna fringilla ultrices. Phasellus eu tellus sit amet tortor gravida placerat. Integer sapien est, iaculis in, pretium quis, viverra ac, nunc. Praesent eget sem vel leo ultrices bibendum. Aenean faucibus. Morbi dolor nulla, malesuada eu, pulvinar at, mollis ac, nulla. Curabitur auctor semper nulla. Donec varius orci eget risus. Duis nibh mi, congue eu, accumsan eleifend, sagittis quis, diam. Duis eget orci sit amet orci dignissim rutrum.

Contents

List of Tables

List of Figures

Chapter 1

Introduction

Ultrasound elastography is a relatively new ultrasonic imaging modality which utilizes traditional ultrasound waveforms to interrogate tissue stiffness rather than tissue echogenicity as is done in classic ultrasound imaging. The resulting tissue stiffness maps are referred to as elastograms, a terminology which will be used throughout this work. By examining displacement characteristics of tissue under load, the relative localized stiffness of the tissue may be ascertained. While regional tissue stiffness changes are to be expected due to the heterogeneous composition of generalized soft tissues, localized stiffness changes may be used as an indicator of tissue health [1] with relatively stiff tissues showing signs of rigor mortis and cell death and relatively soft tissues showing signs of tissue necrosis and decomposition. While ultrasound elastography has typically been used to investigate cancerous lesions this work seeks to use it as a means of detecting deep tissue injuries which as of the time of writing are not clinically detectable until they breach the surface of the skin.

Before ultrasound elastography can be used clinically with any degree of certainty, the effect of numerous important parameters relating to the imaging modality must be understood and characterized. For example, chief parame-

ters of interest include the depth of a lesion and its overall size—parameters which may immediately disqualify certain lesions from even being interrogated by diffused ultrasound beams and as a result would be invisible on the subsequent elastogram. Similarly, for the purposes of designing application-specific elastography transducers it becomes critical to fully understand the effect of transducer device parameters such as ultrasonic probing frequency and transducer f-number on the elastogram icanamage quality and lesion contrast. In order to properly use ultrasound elastography to detect, diagnose, and monitor formative and progressive deep tissue injuries it is crucial to first fully understand and characterize the technology for this specific use.

1.1 Objective

The broad objective of this work was to numerically characterize the use of ultrasound elastography to detect and monitor formative and progressive deep tissue injuries. When the effect of numerous interrogation parameters is understood, the technology may be evaluated on its feasibility and usefulness to detect deep tissue injuries, with the ultimate goal that ultrasound elastography be implemented clinically for detecting deep tissue injuries.

1.2 Motivation

According to the National Pressure Ulcer Advisory Board, deep tissue injuries are classified as a sub-category of pressure ulcers [2]. Pressure ulcers and subsequently deep tissue injuries are commonly suffered by people with limited mobility, such as those undergoing lengthy surgical procedures, the elderly, and those with spinal cord injuries [3] with up to 80 % of people with spinal cord injuries developing at least one pressure ulcer in their lifetime [4]. While

traditional pressure ulcers form in a "top-to-bottom" pattern [??], deep tissue injuries form in a "bottom-to-top" pattern, whereby the injury starts deep below the skin surface—often at the bone-muscle interface [5]. This nature of not being externally visible until the wound has severely progressed makes deep tissue injuries exceedingly difficult to not only diagnose but also to prevent and treat.

As of the time of writing, there is no clinically feasible method of detecting deep tissue injuries until they begin to damage the skin—even the National Pressure Ulcer Advisory Panel's description of them is largely based on their appearance after the fact [6]. With our inability to detect these forming injuries and subsequently implement deep tissue injury prevention and mitigation protocols, the injuries may eventually progress to form large subcutaneous cavities which eventually break through the surface and reveal themselves as stage III or IV pressure ulcers [7, 8].

1.3 Methodology

In order to investigate the use of ultrasound elastography for the detection of deep tissue injuries, the technology must first be characterized and fully understood. While traditional experimentation provides an opportunity to work with physical subjects it can be severely limiting as absolute control over all investigated parameters is relinquished. Further, subject recruitment may present an insurmountable barrier to the execution of such a study. As such, in this exploratory work, various numerical models of the technology have been utilized to investigate the controlled effect of a broad number of parameters relating to each technology. Specifically, finite-element models of ultrasonic wave propagation in heterogeneous soft tissues have been developed. These models

were coupled with various tissue strain estimation algorithms and utilized to carry out parametric studies on the detection sensitivity of ultrasound elastography with respect to various lesion and technological parameters. Chief parameters of interest include those related to the physical realities of deep tissue injuries such as lesion depth, size, and relative mechanical stiffness as well as parameters related to the design and development of appropriate ultrasonic transducers such as probing frequency, transducer f-number, etc.

1.4 Thesis Outline

In this work, three methods of ultrasonic elastogram image formation have been investigated: quasi-static ultrasound elastography, acoustic radiation force impulse imaging, and shear wave speed quantification. While all three methods may be used to interrogate tissue stiffness utilizing the principles of ultrasound physics.

Chapter 2

Literature Review

2.1 Introduction

Lorem ipsum dolor sit amet, consectetuer adipiscing elit. Ut purus elit, vestibulum ut, placerat ac, adipiscing vitae, felis. Curabitur dictum gravida mauris. Nam arcu libero, nonummy eget, consectetuer id, vulputate a, magna. Donec vehicula augue eu neque. Pellentesque habitant morbi tristique senectus et netus et malesuada fames ac turpis egestas. Mauris ut leo. Cras viverra metus rhoncus sem. Nulla et lectus vestibulum urna fringilla ultrices. Phasellus eu tellus sit amet tortor gravida placerat. Integer sapien est, iaculis in, pretium quis, viverra ac, nunc. Praesent eget sem vel leo ultrices bibendum. Aenean faucibus. Morbi dolor nulla, malesuada eu, pulvinar at, mollis ac, nulla. Curabitur auctor semper nulla. Donec varius orci eget risus. Duis nibh mi, congue eu, accumsan eleifend, sagittis quis, diam. Duis eget orci sit amet orci dignissim rutrum.

2.2 Deep Tissue Injuries

Lorem ipsum dolor sit amet, consectetuer adipiscing elit. Ut purus elit, vestibulum ut, placerat ac, adipiscing vitae, felis. Curabitur dictum gravida mauris. Nam arcu libero, nonummy eget, consectetuer id, vulputate a, magna. Donec vehicula augue eu neque. Pellentesque habitant morbi tristique senectus et netus et malesuada fames ac turpis egestas. Mauris ut leo. Cras viverra metus rhoncus sem. Nulla et lectus vestibulum urna fringilla ultrices. Phasellus eu tellus sit amet tortor gravida placerat. Integer sapien est, iaculis in, pretium quis, viverra ac, nunc. Praesent eget sem vel leo ultrices bibendum. Aenean faucibus. Morbi dolor nulla, malesuada eu, pulvinar at, mollis ac, nulla. Curabitur auctor semper nulla. Donec varius orci eget risus. Duis nibh mi, congue eu, accumsan eleifend, sagittis quis, diam. Duis eget orci sit amet orci dignissim rutrum.

2.2.1 Aetiology

Lorem ipsum dolor sit amet, consectetuer adipiscing elit. Ut purus elit, vestibulum ut, placerat ac, adipiscing vitae, felis. Curabitur dictum gravida mauris. Nam arcu libero, nonummy eget, consectetuer id, vulputate a, magna. Donec vehicula augue eu neque. Pellentesque habitant morbi tristique senectus et netus et malesuada fames ac turpis egestas. Mauris ut leo. Cras viverra metus rhoncus sem. Nulla et lectus vestibulum urna fringilla ultrices. Phasellus eu tellus sit amet tortor gravida placerat. Integer sapien est, iaculis in, pretium quis, viverra ac, nunc. Praesent eget sem vel leo ultrices bibendum. Aenean faucibus. Morbi dolor nulla, malesuada eu, pulvinar at, mollis ac, nulla. Curabitur auctor semper nulla. Donec varius orci eget risus. Duis nibh mi, congue eu, accumsan eleifend, sagittis quis, diam. Duis eget orci sit amet orci

dignissim rutrum.

2.2.2 Treatment

Lorem ipsum dolor sit amet, consectetuer adipiscing elit. Ut purus elit, vestibulum ut, placerat ac, adipiscing vitae, felis. Curabitur dictum gravida mauris. Nam arcu libero, nonummy eget, consectetuer id, vulputate a, magna. Donec vehicula augue eu neque. Pellentesque habitant morbi tristique senectus et netus et malesuada fames ac turpis egestas. Mauris ut leo. Cras viverra metus rhoncus sem. Nulla et lectus vestibulum urna fringilla ultrices. Phasellus eu tellus sit amet tortor gravida placerat. Integer sapien est, iaculis in, pretium quis, viverra ac, nunc. Praesent eget sem vel leo ultrices bibendum. Aenean faucibus. Morbi dolor nulla, malesuada eu, pulvinar at, mollis ac, nulla. Curabitur auctor semper nulla. Donec varius orci eget risus. Duis nibh mi, congue eu, accumsan eleifend, sagittis quis, diam. Duis eget orci sit amet orci dignissim rutrum.

2.2.3 Detection

- Derp

2.3 Ultrasound Elastography

Lorem ipsum dolor sit amet, consectetuer adipiscing elit. Ut purus elit, vestibulum ut, placerat ac, adipiscing vitae, felis. Curabitur dictum gravida mauris. Nam arcu libero, nonummy eget, consectetuer id, vulputate a, magna. Donec vehicula augue eu neque. Pellentesque habitant morbi tristique senectus et netus et malesuada fames ac turpis egestas. Mauris ut leo. Cras viverra metus rhoncus sem. Nulla et lectus vestibulum urna fringilla ultrices. Phasellus eu

tellus sit amet tortor gravida placerat. Integer sapien est, iaculis in, pretium quis, viverra ac, nunc. Praesent eget sem vel leo ultrices bibendum. Aenean faucibus. Morbi dolor nulla, malesuada eu, pulvinar at, mollis ac, nulla. Curabitur auctor semper nulla. Donec varius orci eget risus. Duis nibh mi, congue eu, accumsan eleifend, sagittis quis, diam. Duis eget orci sit amet orci dignissim rutrum.

2.3.1 Quasi-Static Ultrasound Elastography

Lorem ipsum dolor sit amet, consectetuer adipiscing elit. Ut purus elit, vestibulum ut, placerat ac, adipiscing vitae, felis. Curabitur dictum gravida mauris. Nam arcu libero, nonummy eget, consectetuer id, vulputate a, magna. Donec vehicula augue eu neque. Pellentesque habitant morbi tristique senectus et netus et malesuada fames ac turpis egestas. Mauris ut leo. Cras viverra metus rhoncus sem. Nulla et lectus vestibulum urna fringilla ultrices. Phasellus eu tellus sit amet tortor gravida placerat. Integer sapien est, iaculis in, pretium quis, viverra ac, nunc. Praesent eget sem vel leo ultrices bibendum. Aenean faucibus. Morbi dolor nulla, malesuada eu, pulvinar at, mollis ac, nulla. Curabitur auctor semper nulla. Donec varius orci eget risus. Duis nibh mi, congue eu, accumsan eleifend, sagittis quis, diam. Duis eget orci sit amet orci dignissim rutrum.

2.3.2 Acoustic Radiation Force Impulse Imaging

Lorem ipsum dolor sit amet, consectetuer adipiscing elit. Ut purus elit, vestibulum ut, placerat ac, adipiscing vitae, felis. Curabitur dictum gravida mauris. Nam arcu libero, nonummy eget, consectetuer id, vulputate a, magna. Donec vehicula augue eu neque. Pellentesque habitant morbi tristique senectus et netus et malesuada fames ac turpis egestas. Mauris ut leo. Cras viverra metus

rhoncus sem. Nulla et lectus vestibulum urna fringilla ultrices. Phasellus eu tellus sit amet tortor gravida placerat. Integer sapien est, iaculis in, pretium quis, viverra ac, nunc. Praesent eget sem vel leo ultrices bibendum. Aenean faucibus. Morbi dolor nulla, malesuada eu, pulvinar at, mollis ac, nulla. Curabitur auctor semper nulla. Donec varius orci eget risus. Duis nibh mi, congue eu, accumsan eleifend, sagittis quis, diam. Duis eget orci sit amet orci dignissim rutrum.

2.3.3 Shear Wave Speed Quantification

Lorem ipsum dolor sit amet, consectetuer adipiscing elit. Ut purus elit, vestibulum ut, placerat ac, adipiscing vitae, felis. Curabitur dictum gravida mauris. Nam arcu libero, nonummy eget, consectetuer id, vulputate a, magna. Donec vehicula augue eu neque. Pellentesque habitant morbi tristique senectus et netus et malesuada fames ac turpis egestas. Mauris ut leo. Cras viverra metus rhoncus sem. Nulla et lectus vestibulum urna fringilla ultrices. Phasellus eu tellus sit amet tortor gravida placerat. Integer sapien est, iaculis in, pretium quis, viverra ac, nunc. Praesent eget sem vel leo ultrices bibendum. Aenean faucibus. Morbi dolor nulla, malesuada eu, pulvinar at, mollis ac, nulla. Curabitur auctor semper nulla. Donec varius orci eget risus. Duis nibh mi, congue eu, accumsan eleifend, sagittis quis, diam. Duis eget orci sit amet orci dignissim rutrum.

2.4 Numerical Characterization / Finite-Element Modelling

Lorem ipsum dolor sit amet, consectetuer adipiscing elit. Ut purus elit, vestibulum ut, placerat ac, adipiscing vitae, felis. Curabitur dictum gravida mauris.

Nam arcu libero, nonummy eget, consectetuer id, vulputate a, magna. Donec vehicula augue eu neque. Pellentesque habitant morbi tristique senectus et netus et malesuada fames ac turpis egestas. Mauris ut leo. Cras viverra metus rhoncus sem. Nulla et lectus vestibulum urna fringilla ultrices. Phasellus eu tellus sit amet tortor gravida placerat. Integer sapien est, iaculis in, pretium quis, viverra ac, nunc. Praesent eget sem vel leo ultrices bibendum. Aenean faucibus. Morbi dolor nulla, malesuada eu, pulvinar at, mollis ac, nulla. Curabitur auctor semper nulla. Donec varius orci eget risus. Duis nibh mi, congue eu, accumsan eleifend, sagittis quis, diam. Duis eget orci sit amet orci dignissim rutrum.

2.5 Conclusion

Lorem ipsum dolor sit amet, consectetuer adipiscing elit. Ut purus elit, vestibulum ut, placerat ac, adipiscing vitae, felis. Curabitur dictum gravida mauris. Nam arcu libero, nonummy eget, consectetuer id, vulputate a, magna. Donec vehicula augue eu neque. Pellentesque habitant morbi tristique senectus et netus et malesuada fames ac turpis egestas. Mauris ut leo. Cras viverra metus rhoncus sem. Nulla et lectus vestibulum urna fringilla ultrices. Phasellus eu tellus sit amet tortor gravida placerat. Integer sapien est, iaculis in, pretium quis, viverra ac, nunc. Praesent eget sem vel leo ultrices bibendum. Aenean faucibus. Morbi dolor nulla, malesuada eu, pulvinar at, mollis ac, nulla. Curabitur auctor semper nulla. Donec varius orci eget risus. Duis nibh mi, congue eu, accumsan eleifend, sagittis quis, diam. Duis eget orci sit amet orci dignissim rutrum.

Chapter 3

Numerical Characterization of Quasi-Static Ultrasound Elastography

3.1 Introduction

Lorem ipsum dolor sit amet, consectetuer adipiscing elit. Ut purus elit, vestibulum ut, placerat ac, adipiscing vitae, felis. Curabitur dictum gravida mauris. Nam arcu libero, nonummy eget, consectetuer id, vulputate a, magna. Donec vehicula augue eu neque. Pellentesque habitant morbi tristique senectus et netus et malesuada fames ac turpis egestas. Mauris ut leo. Cras viverra metus rhoncus sem. Nulla et lectus vestibulum urna fringilla ultrices. Phasellus eu tellus sit amet tortor gravida placerat. Integer sapien est, iaculis in, pretium quis, viverra ac, nunc. Praesent eget sem vel leo ultrices bibendum. Aenean faucibus. Morbi dolor nulla, malesuada eu, pulvinar at, mollis ac, nulla. Curabitur auctor semper nulla. Donec varius orci eget risus. Duis nibh mi, congue eu, accumsan eleifend, sagittis quis, diam. Duis eget orci sit amet orci

dignissim rutrum.

3.2 Method

In order to evaluate the sensitivity of using quasi-static ultrasound elastography to detect deep tissue injuries, a numerical model of these injuries was created such that a subset of the investigated cases mimicked a physical phantom model which was used for validation. This numerical model allowed the rapid modification of numerous parameters related to DTI to examine their effect on the method's detection sensitivity where detection sensitivity is defined as the slope of the given characterization plot. To fully understand the problem, 5 general model cases were studied with each case generating numerous sub-studies on the effect of various parameters relating to that case. These parameters included: lesion depth; lesion altitude (distance of the lesion above deep bone); lesion diameter; ratio of the stiffness between the lesion and the surrounding tissue; ultrasound probing frequency; strain level applied by the transducer; the separation distance between two co-located lesions; radius of a circular averaging filter applied to the lesion boundaries; the number of smaller clustered lesions per unit area; the radius of each individual clustered lesion; the width of the lesion in a Visible Human [9] model and the depth of the lesion in a Visible Human model. The range of values for the tested parameters are given in Table 3.1 which resulted in a total of 144 model cases that were analyzed. The geometry of the models shown in Fig. 3.1 include: a simple spherical lesion embedded within a 2-dimensional rectangular zone of soft tissue; two lesions located at the same depth separated laterally by a finite dimension, δ_{sep}; a spherical lesion without hard boundaries; a cluster of small lesions which together form a larger lesion area; and a lesion with mri-acquired

Table 3.1: Range of values of investigated parameters

Parameter	Symbol	Values
Lesion depth	d	$[3.5, 6.5, 8.5, 10.0]$ cm
Lesion altitude	h	$[1.25, 2.50, 3.75]$ cm
Lesion diameter	$\varnothing S$	$[0.5, 1.0, 2.0, 2.5]$ cm
Lesion stiffness ratio	E_{rel}	$[0.32, 0.56, 1.80, 3.20]$
Ultrasound frequency	f	$[2, 4, 8]$ MHz
Transudcer-applied strain	ε_{app}	$[2.5, 5.0, 10.0]$ %
Colocated separation distance	δ_{sep}	$[1.25, 1.50, 1.75, 2.00]$ cm
Blurred lesion blur radius	b_r	$[1.0, 2.5, 5.0, 7.5]$ mm
Clustered lesion density	b_ρ	$[10, 20, 30, 40]$ cm^{-2}
Clustered lesion radius	r_{bl}	$[0.5, 1.0, 1.5]$ mm
Visible human lesion width	$\varnothing S$	$[0.5, 1.0, 2.0, 2.5]$ cm
Visible human lesion depth	d	$[6.25, 6.75, 7.25]$ cm

geometry [10] embedded in geometry obtained from a Visible Human slice [9].

In Fig. 3.1e, the lesion is located superficial to the left ischial tuberosity in the transverse plane. The lesion geometry was obtained from an MRI scan of a real deep tissue injury induced in a porcine model [10]. The generic soft tissue in this model is modelled after muscle, with a layer of adipose tissue residing at the surface of the model.

Note that the axial direction referred to henceforth as the "axial" direction of an ultrasound transducer placed along the top (superficial) surface of the domain such that it becomes the "vertical" direction.

Simulated ultrasound images were acquired through the convolution of a point spread function with a normally distributed background map of scattering centres [11]. These images were then combined with a finite-element deformation model of the strained tissue to generate both pre- and post- compression images of the lesions and surrounding tissue. These images were fed into a tissue strain estimation algorithm to determine the detection sensitivity of the technique. Finally, the technique was validated against a physical phantom model using a subset of the simulated cases.

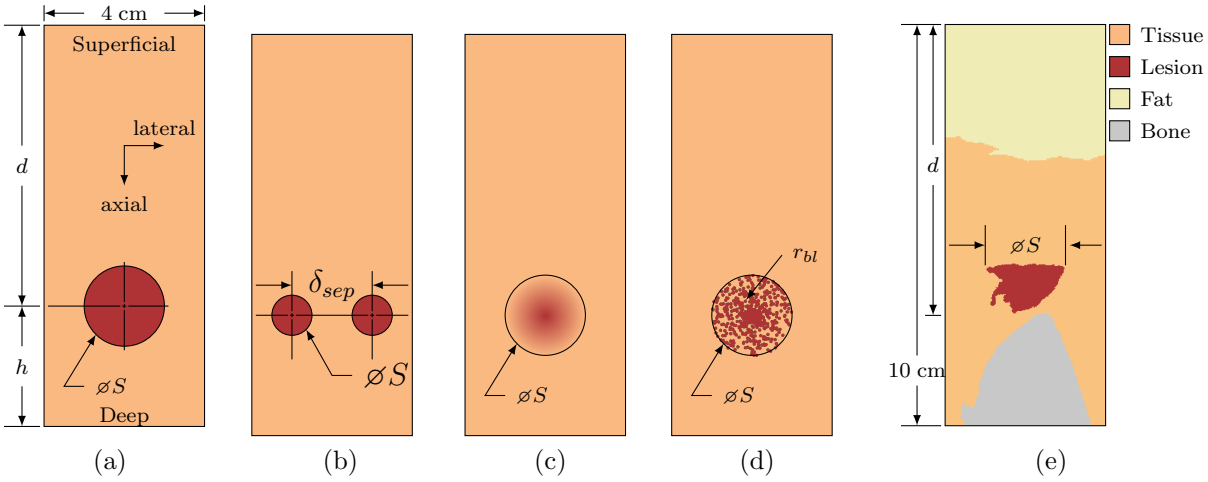

Figure 3.1: Model geometry showing the investigated lesions embedded in a 4 cm wide soft tissue domain. Axial and lateral directions mimic that of a typical ultrasound transducer placed along the top boundary of the domain. The simplest case of a circular lesion embedded in a soft tissue domain located superior to hard underlying bone is shown in (a). In order to investigate the interference caused by closely-located lesions, the case shown in (b) was investigated. Because of the relatively unknown and variable geometric properties of deep tissue injury lesions, cases (c) and (d) were investigated where the lesion edges were blurred and the lesion was actually a large collection of small lesions, respectively. Finally, to investigate detection sensitivity in a realistic setting, case (e) was investigated where an mri-acquired deep tissue injury was overlaid on a slice from the Visible Human Project such that the injury lesion was located immediately superior to an ischial tuberosity.

3.2.1 Formation of B-Mode Ultrasound Images

Through the convolution of a point spread function and a normal random distribution of scattering centres, simulated ultrasound images were generated. The point spread function was defined axially as a cosine function operating at the ultrasound probing frequency modulated by a Gaussian distribution defined by $\mu = 2\lambda$ and $\sigma = 2\lambda$ where λ is the wavelength of the ultrasonic probing waves. Laterally, the point spread function was modelled as a Gaussian distribution defined by $\mu = 0$ and $\sigma = 0.25w_{active}$ where w_{active} is the total width of the active transducer elements during scan-line acquisition. This resulted in the point spread function given in Fig. 3.2. Resulting images were

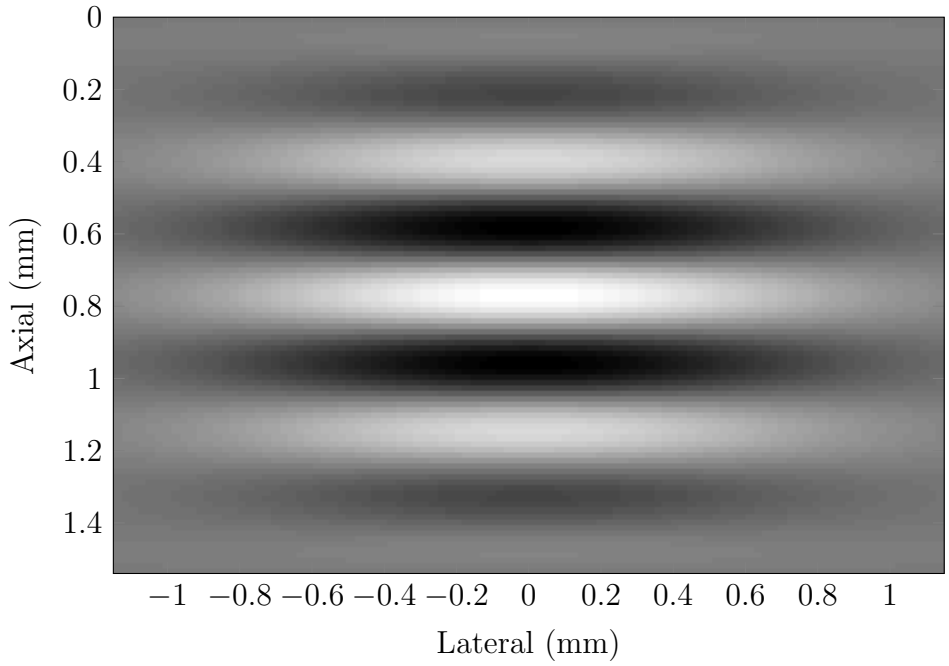

Figure 3.2: Point spread function used for simulating b-mode ultrasound scans. The function is defined axially by a cosine function at the probing frequency and modulated by a Gaussian function both axially and laterally.

composed of 192 scan lines each sampled at 50 MHz.

3.2.2 Finite-Element Model of Tissue Deformation Under Surface Distortion

As a response to an external load being applied to the boundary of a domain, internal structures deform. In the case of a relatively stiff deep tissue injury embedded within surrounding soft tissues, this implies that when the surface of the skin is depressed, the relatively stiff lesion will not strain to the same magnitude that the surrounding soft tissue does. In order to simulate the deformation of interrogated tissue, the displacement field for the simulated models was calculated according to:

$$-\nabla \cdot \sigma = F \tag{3.1}$$

Where σ is the Cauchy stress tensor and F are the applied body forces. Simulations were performed assuming a 2-dimensional linearly elastic material deformation model under plane strain conditions. A 3-dimensional model was also considered, however the deformations differed from the 2-dimensional simulation by less than 1 % so a 2-dimensional model was deemed adequate. Soft tissue was modelled using a Young's modulus of elasticity of 25 kPa, Poisson's ratio of 0.499, and density of 998 kg/m^3 [12, 13, 14]. The only difference in lesion mechanical properties from the surrounding soft tissue was the modulus of elasticity which varied according to the simulation parameters. The bottom of the domain was held fixed such that:

$$u = 0, \qquad \Gamma = \Gamma_{bottom} \tag{3.2}$$

While this boundary condition represents an idealized scenario, it may be likened to that of tissue located superficial to a relatively stiff anchoring bone below. This lower region is where deep tissue injuries generally form and is therefore of special importance. Compressive strains were applied to the top of the domain so as to induce strain along the top boundary:

$$u = (0, -u_0), \qquad \Gamma = \Gamma_{top} \tag{3.3}$$

From these simulations, displacement fields throughout the domain were calculated which were then used to displace tissue (including scattering centres) in the simulated ultrasound images in both the axial and lateral directions. This process resulted in pairs of pre- and post- compression simulated b-mode images of lesions of varying parameters which could then be analyzed and characterized.

3.2.3 Characterizing Quasi-Static Ultrasound Elastography

Utilizing a 2-D locally regularized tissue strain estimation algorithm [15], pairs of pre- and post- compression images were used to calculate elastogram estimations for the full range of parameter values of the simulated lesions. The algorithm consists of sweeping the image domain with a series of overlapping regions of interest (ROI). ROI are compared between pre- and post- compression images, with ROI in the post- compression images being axially scaled and translated and laterally translated versions of the same ROI in the pre-compression images.

Qualitatively, the noise and computation time of the resulting elastograms were found to be minimum when using an axial ROI size of approximately 10 times the ultrasound wavelength. Axial ROI overlap was held at 99 % to produce elastograms with minimal noise, even though this introduced significant increases in computation time. Due to the extreme anisotropic nature of ultrasound signals, lateral ROI size was kept to 5 signal widths with lateral ROI overlaps of 80 %.

3.2.4 Model Validation Using a Commercially Available Phantom

Utilizing a CIRS Elasticity QA Phantom model 049, a subset of the results obtained from the finite-element simulations and numerical characterizations were compared against their physical phantom equivalents. The phantom mimics acoustically homogeneous soft tissue with embedded lesions which vary in depth, size, and mechanical stiffness. Mechanical properties of the phantom as given by manufacturer specifications are summarized in Table 3.2. Pre- and

Table 3.2: CIRS Phantom Model Mechanical Properties

Property	Value
Nominal basal stiffness	25 kPa
Lesion stiffness	$[8, 14, 45, 80]$ kPa
Speed of sound	1540 m/s
Acoustic attenuation	0.5 dB/cm MHz
Lesion diameter	$[10, 20]$ mm
Lesion depth	$[15, 35]$ mm

post- compression b-mode ultrasound images were obtained of each lesion in the phantom and the resulting strain ratio for that lesion was compared to the simulated strain ratio for that combination of parameters. Specifically, lesions at a depth of 3.5 cm, a diameter of 2.0 cm, and with true stiffness ratios of 0.56, 1.80, and 3.20 were examined. Surface indentation was performed manually with the transducer indenting approximately 0.5 cm (6.25 %) at the surface.

3.3 Results

Following the procedure outlined in Section 3.2, finite-element models of ultrasonic b-mode image formation and tissue deformation were synthesized. The results of these models were then fed into the local strain estimation algorithm described in Section 3.2.3. The resulting numerical characterizations of the relationship between measured and true strain ratios in the simulated tissue and their dependence on the various lesion parameters given in Table 3.1 were examined. Finally, the local strain estimation algorithm was carried out on a physical phantom and compared against a subset of the simulated cases.

3.3.1 Finite Element Models of Ultrasound and Deformation

Sample images generated using both the acoustic and deformation finite-element models are given in Figs. 3.3a, 3.3b and 3.3c. In Fig. 3.3a, a sample generated b-mode ultrasound scan is given. Fig. 3.3b shows the vector-sum displacement field generated by the deformation finite-element model. The entire top surface of the model has been displaced axially by 6.25 mm (5 %), which caused deformation of both the soft tissue and embedded lesion within. Since the lesion was modelled as being 3.2 times stiffer than the surrounding tissue, the lesion underwent less strain which consequently resulted in the lesser displacement depicted. Fig. 3.3c shows the resultant b-mode image generated by applying the displacement field given in Fig. 3.3b to the tissue and embedded scattering centres used to create Fig. 3.3a. What results is a locally scaled and translated version of Fig. 3.3a that corresponds to indenting the surface of the skin above a stiff lesion. The large anechoic region located at the bottom of the domain is tissue that was not modelled in the pre-compression image as it was outside of the original domain. This area represents the region of tissue that is undetectable with the strain-estimation algorithm given in Section 3.2.3 as the information contained there is only available in one of the two input images and so is considered incomplete data.

3.3.2 Resulting Elastograms

The 2-D locally regularized tissue strain estimation algorithm described in Section 3.2.3 was used in combination with the simulated resultant b-mode ultrasound images (Figs. 3.3a and 3.3c) in order to generate elastogram images which were used in the subsequent analysis. An example elastogram resulting

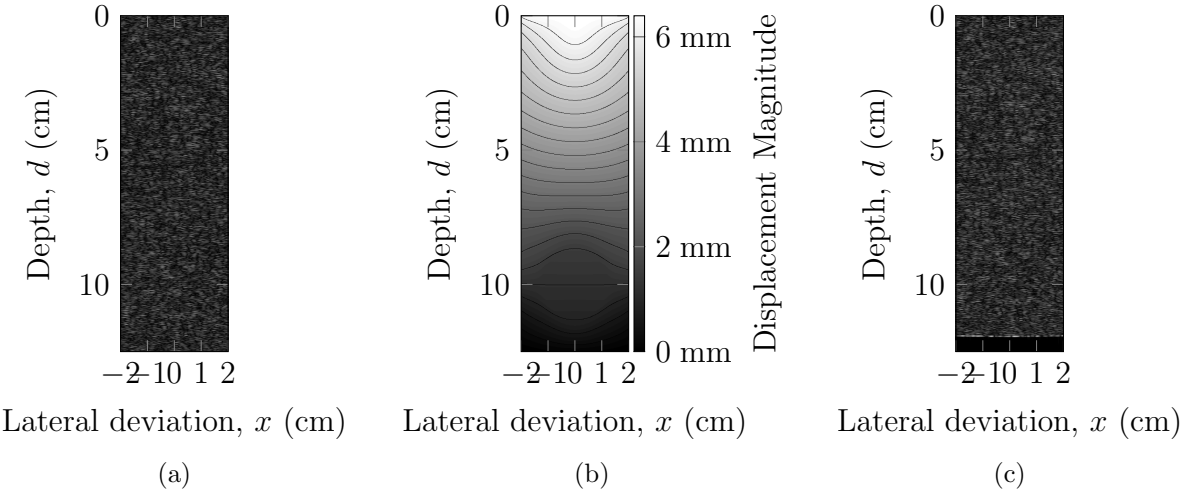

Figure 3.3: Finite-element model results for the case when $d = 10$ cm, $\varnothing S = 2.5$ cm, $\varepsilon_{rel} = 3.20$, and $f = 4$ MHz showing (a) a generated b-mode image of the pre-compressed tissue domain, (b) the vector-summed displacement field induced by compressive strain applied to the top of the boundary, and (c) a generated b-mode image of the post-compressed tissue domain. The included lesion is not visible in (a) and (c) as it's acoustic properties were no different than surrounding tissues. An anechoic region is visible along the bottom of the domain in (c) which represents tissue outside of the domain visible in (a).

from the simulation presented in Fig. 3.3 is shown in Fig. 3.4. Throughout the entire domain on this sample elastogram, regions outside of the stiff lesions showed compressive strains of approximately 5 % as expected due to the compression applied to the upper boundary of the model. The entire lesion region showed relatively consistent low strain amounts of approximately 2.5 %, which is consistent with the lesion being stiffer (and so straining less) than the surrounding tissue. Of note is the increased strain pattern which appeared both axially and laterally around the lesion. While generally symmetric about the axial direction, this stress field was largely concentrated above the lesion when the lesion was deep (close to the bone). This may be explained as a stress concentration brought about by the sudden change in mechanical material properties of the tissue and may serve to fuel the conditions of excessive cell deformation and ischemia which initiated the formation of a deep tissue

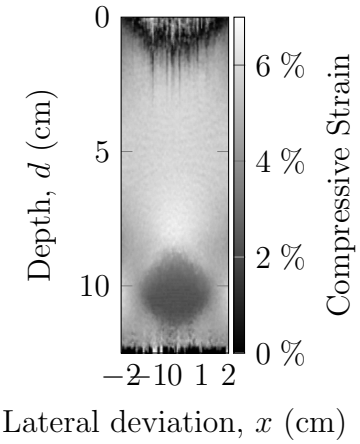

Figure 3.4: Sample strain elastogram showing estimated strain values for $d = 10$ cm, $\varnothing S = 2.5$ cm, $\varepsilon_{rel} = 3.20$, $f = 4$ MHz. While undetectable on a single b-mode image, the elastogram clearly shows a low-strain (stiff) lesion located approximately 10 cm from the surface.

injury in the first place, exacerbating the wound and assisting its expansion toward the surface.

3.3.3 Numerical Characterizations

In order to determine the sensitivity of using quasi-static ultrasound elastography to detect deep tissue injuries, elastograms such as the example that was calculated in Section 3.3.2 were calculated for the full range of parameters given in Table 3.1. "Measured" strain ratios for each elastogram were obtained by comparing the mean strain within each lesion with the mean engineering strain of the surrounding tissue such that:

$$\varepsilon_{rel,measured} = \frac{\varepsilon_{tissue}}{\varepsilon_{lesion}} \tag{3.4}$$

ε_{tissue} was sampled as the mean strain in the region of tissue with the same geometry as the lesion located immediately superficial to the lesion in all cases.

In order to characterize how each parameter of interest affects the detection

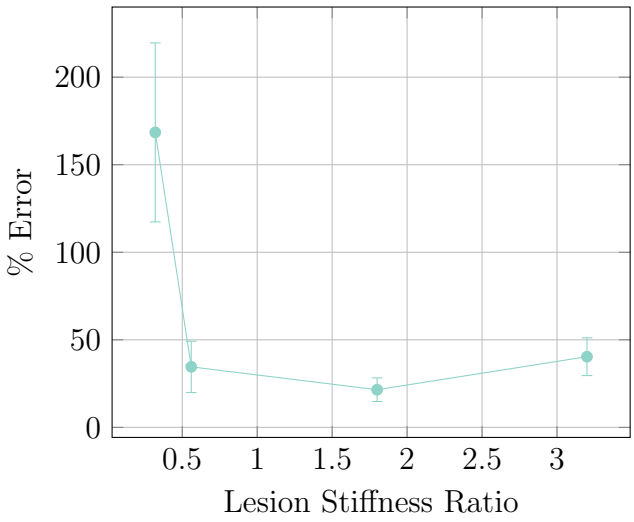

Figure 3.5: Detection ability as it related to true lesion stiffness ratio. For all but small lesion stiffness ratios (very soft "lesions"), results are linear and predictable. For small lesion stiffness ratios (0.32), the lesion becomes severely misrepresented. This is likely due to the algorithm "losing track" of scattering centers for the relatively large displacements induced in the signiciantly less stiff tissue.

sensitivity of quasi-static ultrasound elastography, measured strain ratios for various lesions were calculated and compared against $\varepsilon_{rel,true}$. $\varepsilon_{rel,true}$ is derived from the relative Young's modulus of elasticity of the lesion such that:

$$\varepsilon_{rel,true} = \frac{\varepsilon_{tissue}}{\varepsilon_{lesion}} = \frac{\left(\frac{\sigma_{applied}}{E_{tissue}}\right)}{\left(\frac{\sigma_{applied}}{E_{lesion}}\right)} = \frac{E_{lesion}}{E_{tissue}} \tag{3.5}$$

Fig. 3.5 portrays the severe error involved with using the methods described in Section 3.2 to investigate extremely low stiffness lesions. In nearly all investigated cases where the true lesion stiffness ratio was 0.32, the algorithms described severely misrepresented the measured strain ratio of the lesion, often portraying these extremely low stiffness regions as being more stiff than they truly were. It is hypothesized that the excessively large localized deformations in these lesions interrupted the algorithm's ability to sufficiently track the displacement of scattering centres within the tissue, lowering the

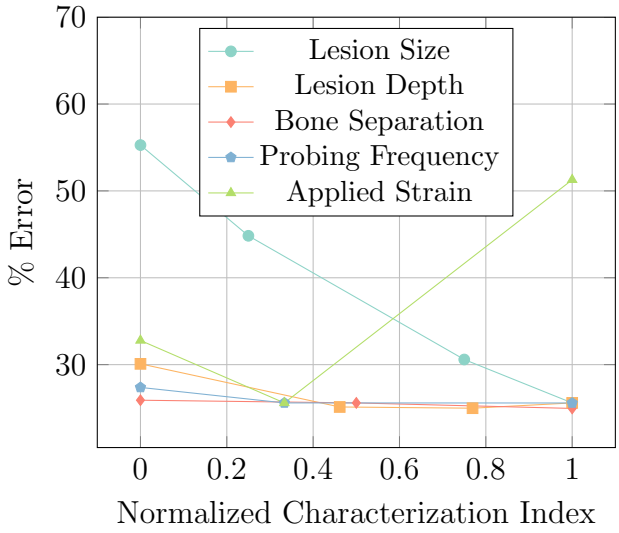

Figure 3.6: Error characterization for range of studied parameters for the simple model of a spherical lesion embedded within soft tissue as seen in Fig. 3.1a. Each parameter has been normalized to the range studied so overly-sensitive regions may be readily distinguished.

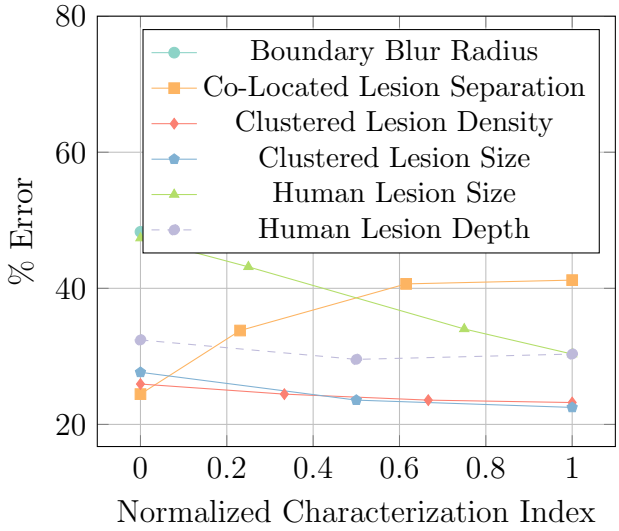

Figure 3.7: Error characterization for range of studied parameters for the co-located lesions, blurred boundary lesions, clustered lesions, and visible human lesion models as seen in Figs. 3.1b – 3.1e. Each parameter has been normalized to the range studied so overly-sensitive regions may be readily distinguished.

magnitude of displacement within the lesion and subsequently increasing it's "measured" strain ratio.

In order to broadly investigate the critical parameter-values of the inves-

tigated models, each parameter was normalized to it's investigated range and the error resulting over these ranges is given in Figs. 3.6 and 3.7.

In Fig. 3.6, it is clear to see that the most sensitive error-inducing situations occur when either the lesion is very small or if large strains are used to deform the tissue. Similarly, it is expected that if the lesion depth were increased much further, significant errors would arise with increasing depth. Logically, this may be explained due to the decreasing magnitude of displacement with increasing depth — at a certain point, the magnitude of displacement of scattering centres will be on par with the measurement noise, and the lesion will cease to be detectable.

From Fig. 3.7 it can be seen that small lesions in the Visible Human-MRI model as well as co-located lesions with large separation distances produce greater measurement errors. Conversely, lesion depth in the Visible Human-MRI model; lesion density and individual lesion size in the clustered lesion model; and boundary blur radius in the blurred-edges model do not seem to affect the measurement error significantly. Of note is the relative large amount of static error present in the boundary blur radius model which is hypothesized to be due to lesser mean tissue stiffness in the investigated region than expected.

Fig. 3.8 shows the relationship between lesion size and detection sensitivity for lesions at a depth of 10 cm in a model depth of 12.5 cm interrogated at 4 MHz with 5 % applied strain. Specifically, Fig. 3.8 shows the decreasing detection sensitivity with decreasing lesion size with the best detection sensitivity being with the largest investigated lesions with a diameter of 2.5 cm. On the opposite end, the detection sensitivity of lesions at or below 0.5 cm in diameter is questionable. This level of detection ability (with regards to lesion size) is acceptable, however, as although there is little data on the true size of

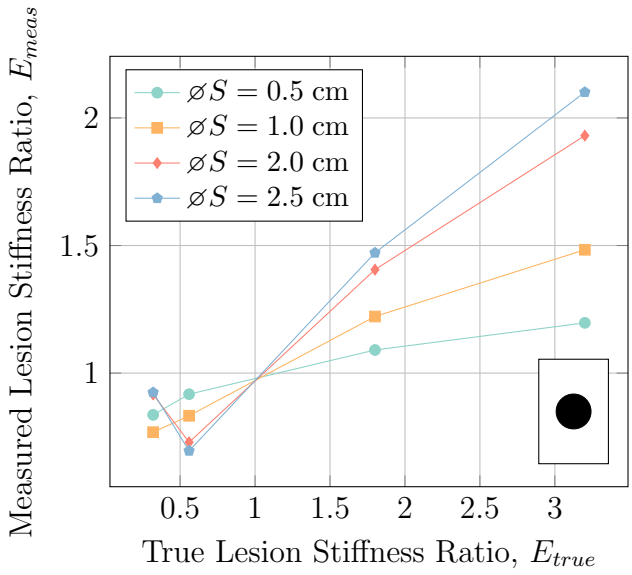

Figure 3.8: Lesion size characterization at a depth of 10 cm with a 4 MHz ultrasound probing frequency showing increasing detection sensitivity of the lesion with increasing lesion size. Detection sensitivity is less than ideal for all cases, with the best case being for lesions approximately 2.5 cm in diameter.

formative DTI, MRI results indicate that untreated deep tissue injuries are on the scale of multiple cm [10]. Thus, being able to detect lesions of at least 1 cm in diameter should prove to be adequate to both detect and monitor DTI.

In order to investigate the effect of lesion depth on the detection sensitivity, measured strain ratios for circular lesions with a diameter of 2.5 cm located at various depths were interrogated with a 4 MHz probing frequency, and strained by 5 %. The results of this investigation are seen in Fig. 3.9.

In Fig. 3.21, it can be seen there there was little interplay between detection sensitivity and measured strain ratios at the various depths examined for all but the case for very soft (mushy) lesions (with a stiffness ratio of 0.32). At such low stiffness ratios, the excessive tissue deformation interrupts the tissue strain estimation algorithm's ability to adequately track the induced displacements in the lesion.

Since the strain field caused by compressive forces near an extremely rigid

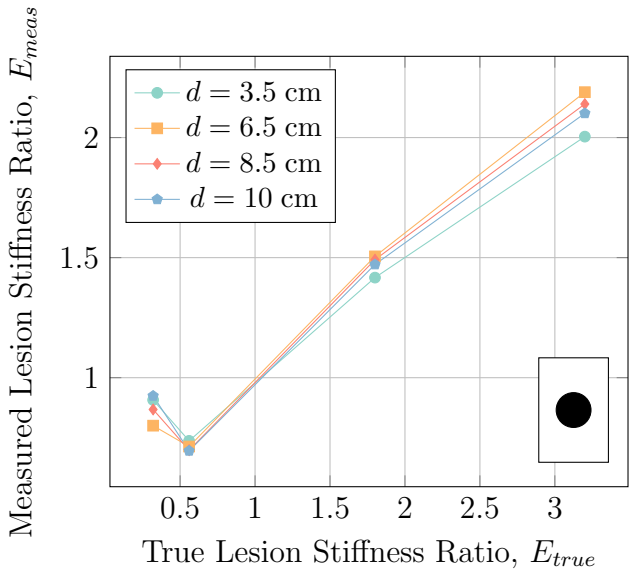

Figure 3.9: Lesion depth characterization at a lesion diameter of 2.5 cm with a 4 MHz ultrasound probing frequency generally showing general independence of detection sensitivity on lesion depth in the tissue.

structure embedded within a relatively soft domain will be significantly heterogeneous, the effect of lesion altitude above the underlying stiff bone was examined with the hypothesis that if the lesion were too close to the hard bone, it would be masked by the strain field caused by the bone's existence. A 2.5 cm diameter lesion was interrogated with a 4 MHz probing frequency and 5 % applied strain. The results of this characterization are given in Fig. 3.10.

In Fig. 3.10, it can be seen that the lesion altitude above the underlying bone had very little effect on the detection sensitivity. Although larger strain fields may be generated near the bone, it is hypothesized that the larger fields also extend larger and so affect healthy tissue to more or less the same degree as the forming lesion.

In order to characterize the effect of using alternate ultrasound probing frequencies, simulations were carried out on lesions using probing frequencies of 2 MHz, 4 MHz, and 8 MHz. The simulated lesions had a diameter of 2.5 cm, were located at a depth of 10 cm and we strain at 5 %. The results of this

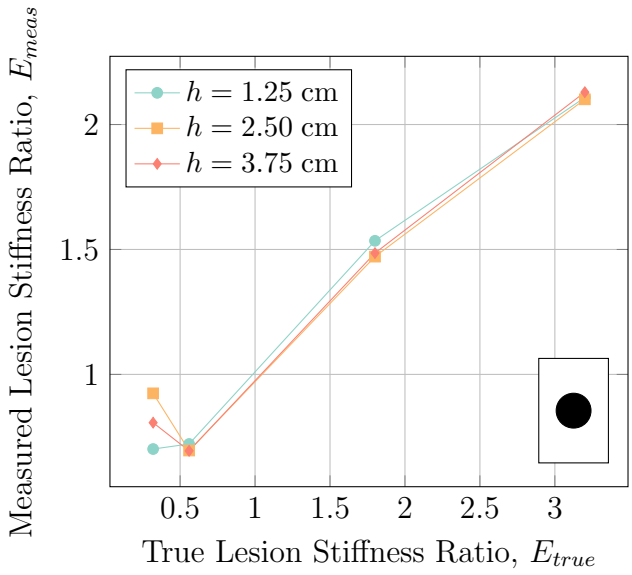

Figure 3.10: Effect of lesion altitude above the underlying bone. Aside from erroneous results at very low lesion stiffness ratios, the effect is negligible.

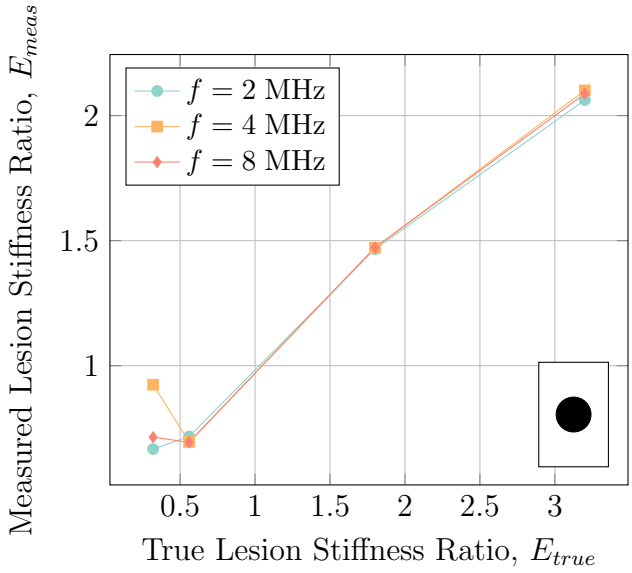

Figure 3.11: Characterization of ultrasonic probing frequency on detection sensitivity. Apart from the requirement of using an ultrasonic frequency low enough to interrogate the desired tissue, probing frequency has negligible effect on the detection sensitivity.

study are given in Fig. 3.11.

As can be seen from Fig. 3.11, there is very little effect on the detection sensitivity from the ultrasound probing frequency that was used, therefore an

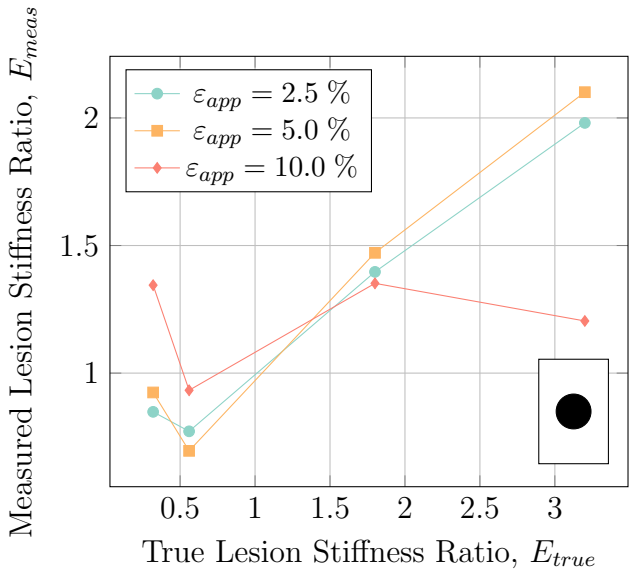

Figure 3.12: Applied strain characterization plot for lesions with a diamater of 2.5 cm located at a depth of 10 cm interrogated at 4 MHz. There is little difference between 2.5 % and 5.0 % applied strain, while large-magnitude strains of 10 % generate significant error for both very soft and very stiff lesions.

appropriate frequency should be chosen so as to reach the the full depth of the bone-muscle interface at suspected DTI locations while retaining the best image resolution.

As quasi-static ultrasound elastography is most likely to be performed via manual indentation where the exact magnitude of applied deformation is unknown, it is important to study the effect of applied strain magnitude on the detection sensitivity. Applied strains of 2.5 %, 5.0 %, and 10 % were investigated on a 2.5 cm diameter lesion at a depth of 10 cm using a probing frequency of 4 MHz; the results are given in Fig. 3.12.

While Fig. 3.12 shows a relatively constant detection sensitivity for compressive strains of 2.5 % and 5 %, compressive strains of 10 % generate significant measurement error for both very soft and very stiff lesions. Under large compressive strains, the tissue (either in the lesion as in the soft lesion case, or the surrounding tissue as in the stiff lesion case) deforms considerably which

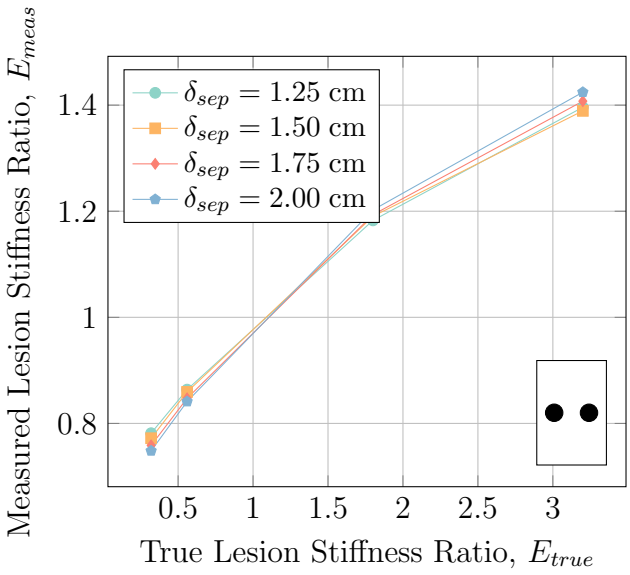

Figure 3.13: Effect of lesion separation distance on two 1.0 cm diameter lesions co-located at a depth of 10 cm interrogated with a 4 MHz probe with 5 % applied strain. There is no negligible difference between separation distances on the detection sensitivity.

again interferes with the algorithm's ability to properly track the displacement of tissue. It should also be noted that applying overly large strains to an already forming deep tissue injury may cause additional unwarranted damage. Thus it is imperative that applied surface indentation be kept to reasonable bounds ($2.5 - 5$ %, or $0.25 - 0.50$ cm in 10 cm deep domains), not only for safety of the tissue but also for clarity of the diagnostic test.

To study the effect that closely spaced lesions will have on the detection sensitivity as well as how discernible the lesions will be from each other, the separation distance between two 1.0 cm diameter co-located lesions at a depth of 10 cm was examined using a 4 MHz probing frequency with 5 % applied strain magnitude. The results of this study are shown in 3.13.

While Fig. 3.13 shows that the separation distance between co-located lesions causes a negligible effect on the detection sensitivity, Fig. 3.14 shows regions of decreased strain above and below the centreline of the lesions. While

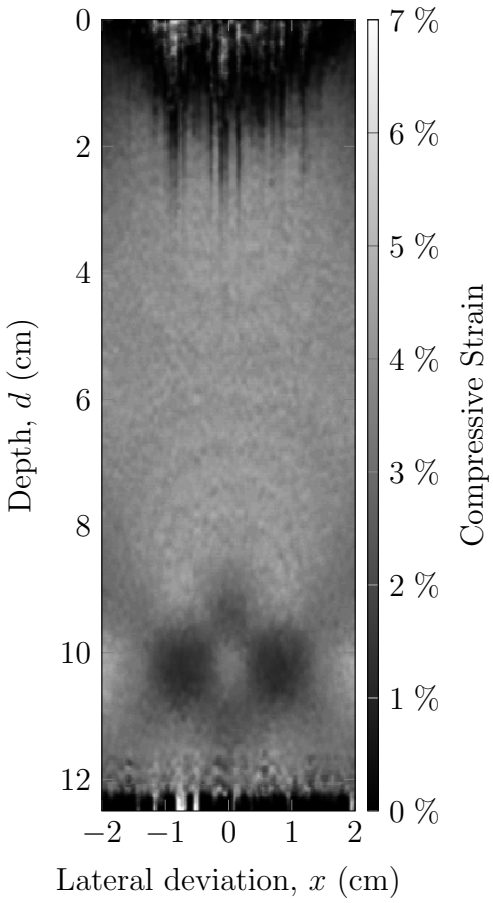

Figure 3.14: Elastogram for two co-located lesions of 1.0 cm diameter at a depth of 10 cm interrogated using a 4 MHz probing frequency with 5 % applied strain. A pattern of decreased strain is present above and below the centerline between the two lesions while the lesions themselves are not affected by each other.

these regions had the same basal stiffness as the bulk tissue, the decreased strain pattern may obfuscate the true results by introducing "phantom lesions" which are not actually present but merely the result of the existing lesions.

While the simulations performed thus far assumed that lesions were perfect spheres with hard boundaries in order to isolate specific parameters of interest, this assumption may not always be accurate. Rather, due to the nature of injury formation, lesions may form gradual boundaries that "fade" from stiff or necrotic tissue to healthy tissue. To investigate the effect of this phenomenon on the detection sensitivity, lesions with "blurred boundaries" were investi-

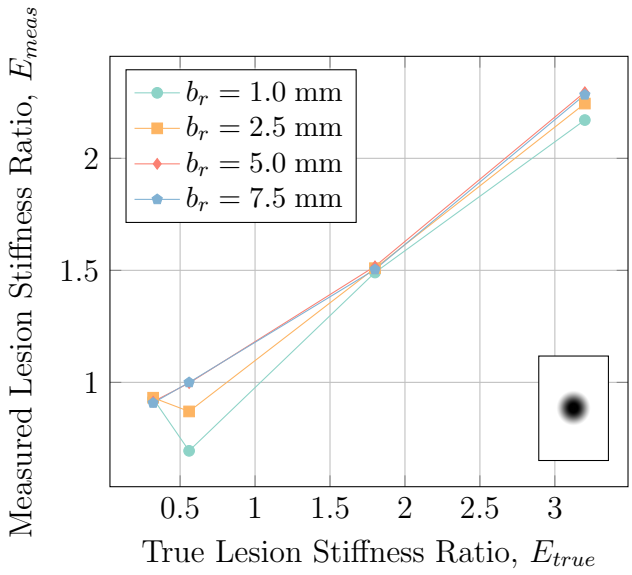

Figure 3.15: Characterization of the effect of lesion blur radius on lesion detection sensitivity for a 2.5 cm diameter lesion at a depth of 10 cm using a probing frequency of 4 MHz and applied strain of 5 %. While there is negligible effect of the blur radius on stiff lesions, the strain ratio for soft lesions is considerably over-estimated.

gated. Hard spherical lesions were blurred by convolving the lesion domain with a disc blurring kernel of varying radius. The results for this investigation on lesions with a diameter of 2.5 cm, at a depth of 10 cm and interrogated with a 4 MHz probing frequency with 5 % applied strain are given in Fig. 3.15.

Fig. 3.15 shows that there is very little dependence on the lesion detection sensitivity for stiff lesions (lesions with a stiffness ratio ≥ 1.0). However, for soft lesions, the tissue strain estimation algorithm seems to over-estimate the stiffness of the lesions.

Similar to how lesions may have "blurred boundaries" rather that hard ones, so too may lesion composition not be homogeneous. In order to study the effect of heterogeneous regions of injured tissue, the detection sensitivity of a set of numerous small lesions located within close proximity to each other so as to form a large, heterogeneous area of diseased tissue was examined. Fig. 3.16 shows the results for this model for varying numbers of 2 mm diameter

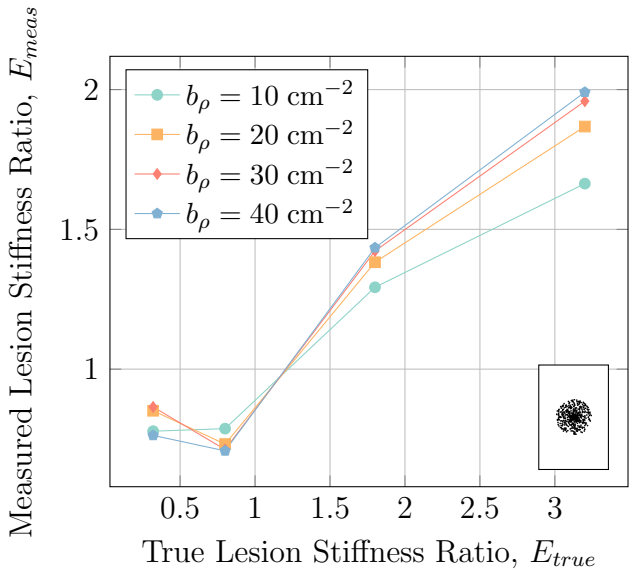

Figure 3.16: Characterization of lesion density for a group of numerous smaller 2 mm diameter lesions comprising a large area with a diameter of 2.5 cm at a depth of 10 cm interrogated with a 4 MHz probing frequency and 5 % applied strain. Detection sensitivity decreases with decreasing lesion density, as expected.

lesions in a 2.5 cm diameter circle located at a depth of 10 cm with a probing frequency of 4 MHz and 5 % applied strain. Fig. 3.18 further explores this model by investigating the case where there are 30 small lesions per square cm with individual lesions ranging in diameter from 0.5 mm to 1.5 mm.

The characterization plot in Fig. 3.16 for small lesion density is less linear than other characterization plots, with lesion density having a significant effect on the detection sensitivity. Specifically, for low lesion densities, the detection sensitivity is much lower than for high lesion densities. However, this observation is warranted after examination of the elastogram produced from these results, given in Fig. 3.17, which shows how the small lesions are not individually detected but rather the entire region is detected as one large lesion. Since the average stiffness ratio over this region is lesser than the stiffness ratio of individual lesions, it makes sense that the "measured" strain ratio will be less than expected.

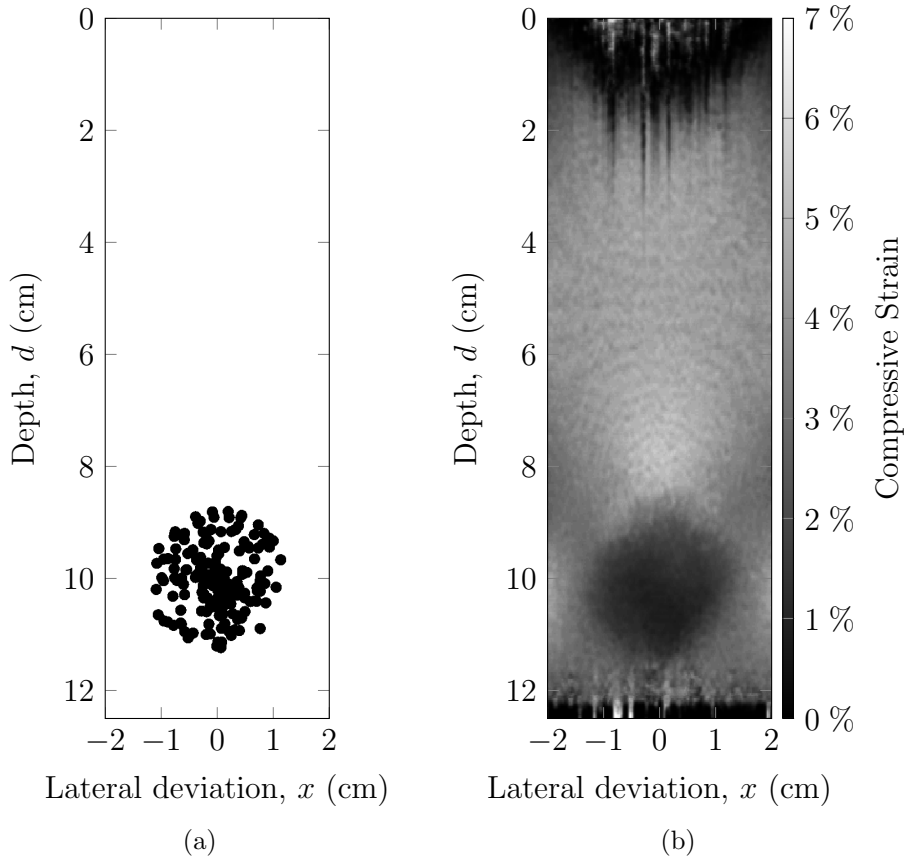

Figure 3.17: Stiffness map (a) and corresponding elastogram (b) for a group a small lesions with a density of 10 lesions per cm^2 grouped in a 2.5 cm diameter circle at a depth of 10 cm interrogated with a 4 MHz probing frequency and 5 % applied strain. In (a), white regions are regular tissue while black regions are the small lesions. In the elastogram, individual lesions do not stand out, rather the entire region of lesions appears as one large region of unhealthy tissue.

Similar to the results shown in Fig. 3.16, changing the size of the individual small lesions does have an effect on the measured strain. In this case, when individual lesions are small, the total area occupied by lesions is lesser which results in a lesser average tissue stiffness over the grouped lesion region.

Note that although the elastography algorithm was able to detect the larger lesion-filled regions in these simulations, it was completely unable to discern the individual lesions comprising those regions. This is not surprising due to both the generated strain fields in the healthy tissue throughout the larger

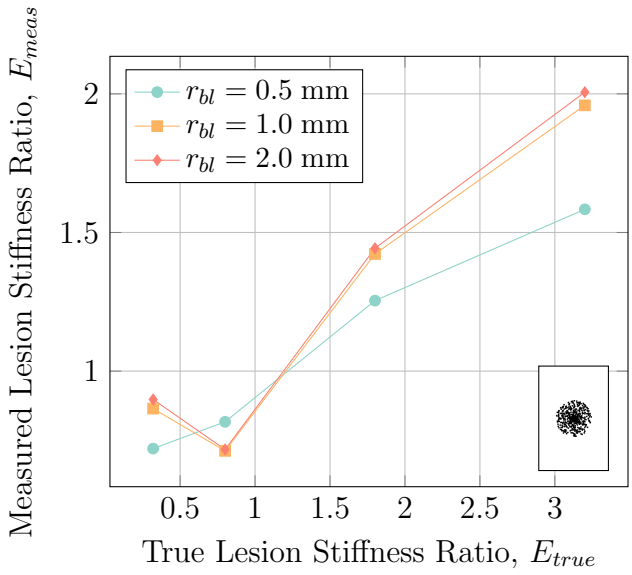

Figure 3.18: Characterization of lesion radius for a group of numerous smaller lesions with a density of 30 lesions per cm^2 comprising a large area with a diameter of 2.5 cm at a depth of 10 cm interrogated with a 4 MHz probing frequency and 5 % applied strain. Detection sensitivity decreases with decreasing individual lesion size, as expected.

lesion area as well as the results presented in Fig. 3.8 showing poor detection sensitivity for lesions with diameters $\leq$ 1 cm while the individual lesions in this simulation had diameters of the scale of 0.5 mm – 1.5 mm.

Finally, in order to place these results within the context of a likely real scenario in humans, a more complicated model utilizing an MRI-acquired lesion and slides from the Visible Human Project [9] was developed. Specifically, lesion geometry was taken from a real deep tissue injury in a pig model imaged using T_2^*-weighted MRI. The human geometry was taken from a transverse plane slice aross the left ischial tuberosity such that the lesion was placed immediately superficial to the boney promience. For this model, the overall lesion width and lesion depth were examined with results shown in Figs. 3.19 and 3.21 respectively.

In Fig. 3.19, it is clear to see than small lesions (with a diameter $\leq$ 1.0 cm) are almost impossible to adequately detect (although larger lesions will be

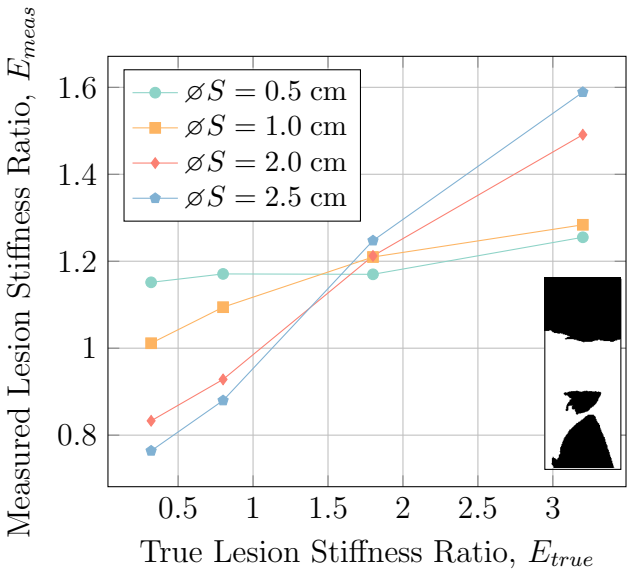

Figure 3.19: Characterization of lesion width in a Visible Human-MRI model for lesions at a depth of 7.25 cm interrogated with a 4 MHz probing frequency with 5 % applied strain. Small lesions (with a width $\leq$ 1.0 cm) are severely misrepresented and portray general over-estimation of lesion stiffness larger lesions.

adequately detectable). It is hypothesized that this phenomenon is due to the excessive strain apparent above the boney prominence that is seen in the resultant elastogram given in Fig. 3.20 such that the lesion is "washed out" by the strain field developed by the relatively stiff bone nearby.

In Fig. 3.21, there is little to no dependence of the detection sensitivity on the lesion depth in the Visible Human-MRI model with all depth curves displaying the same profile. However, deeper lesions (lesions closer to the bony prominence) have stiffnesses that are over-estimated with respect to their superficial counterparts. This is hypothesized to be due to the increased strain field present in all of the soft tissue located immediately superior to the bony prominence, but should not pose a serious problem for imaging lesions of this nature.

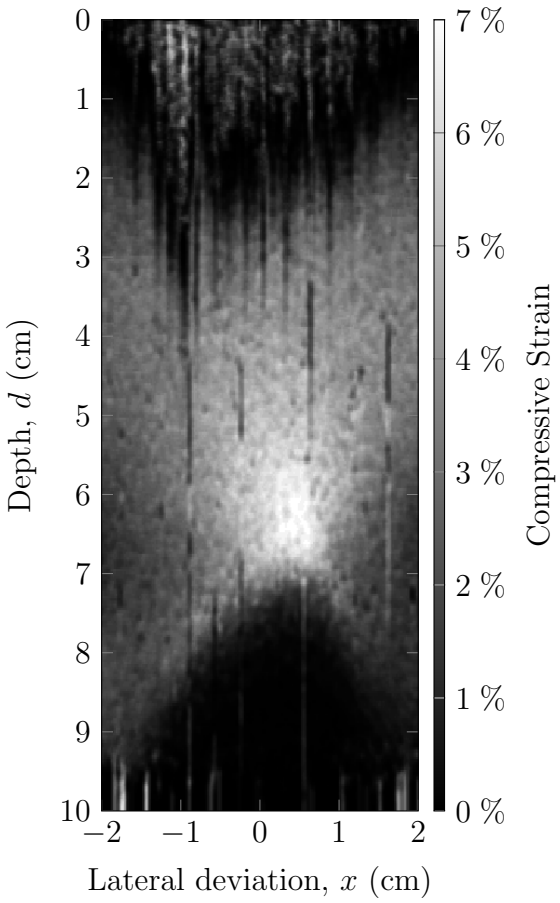

Figure 3.20: Elastogram for a 0.5 cm wide lesion embedded in the Visible Human-MRI model domain at a depth of 7.25 cm interrogated at 4 MHz with an applied strain of 2.5 %. The lesion is not visible and is the resultant elastogram.

3.3.4 Physical Phantom Validation

In order to ensure that the models presented here represented physical realities, a small subset of the cases studied were modelled in a physical phantom, specifically for three lesions with stiffness ratios of 0.56, 1.80, and 3.20 with a diameter of 2.0 cm and at a depth of 3.5 cm, interrogated at 8 MHz with approximately 5 % applied strain. The results of this study are summarized in Fig. 3.22.

As can be seen in Fig. 3.22, a relatively simple (although inexact) relationship between simulated and experimental measured strain ratios exists. It

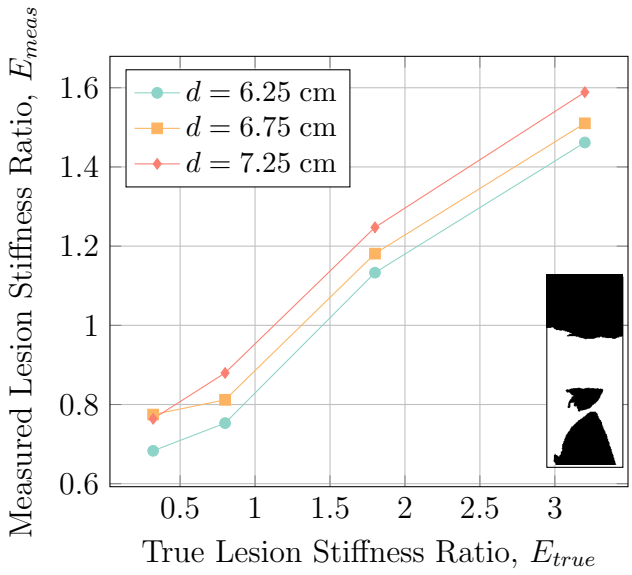

Figure 3.21: Characterization of lesion depth in a Visible Human-MRI model for lesions with a width of 2.5 cm interrogated with a 4 MHz probing frequency and 5 % applied strain. Deeper lesions (closer to the bony promience) are have slightly over-estimated lesion stiffness ratios as opposed to more superficial lesions while detection sensitivity is not affected by lesion depth.

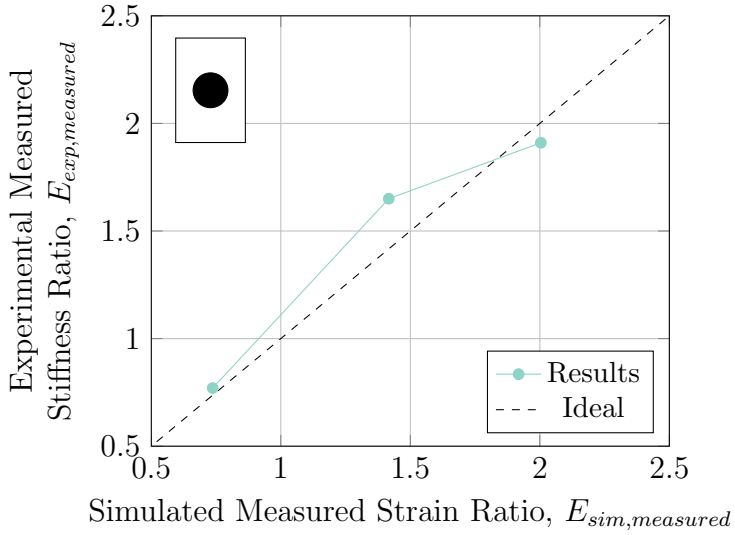

Figure 3.22: Relation between simulated measured strain ratios and experimental measured strain ratios for a lesion at a depth of 3.5 cm and diameter of 2.0 cm showing general agreement between simulated and experimental cases. Idealization errors are the most likely the cause of the differences seen between simulated and experimental cases.

must be noted that the finite-element simulations of b-mode image formation and tissue deformation presented here are idealizations of reality and idealization errors such as the ultrasound pulse profile and plane-strain assumption no doubt contributed to the difference seen in Fig. 3.22.

It must be noted that in order to acquire quasi-static elastography results in the physical phantom, the ultrasound transducer was required to be manually manipulated to cause indentation in the phantom, as the technique would most likely be performed in a clinical setting. This was found to be problematic as the ultrasound transducer was difficult to maintain perfectly perpendicular and in-plane during the compression (largely due to the necessity of using coupling ultrasonic gel). This difficulty suggests that acoustic radiation force impulse (ARFI) elastography would be a more appropriate method to acquire DTI elastograms. ARFI elastography works on the same principles as quasi-static elastography with the exception that tissue deformation is caused by localized large-amplitude acoustic waves generated by the transducer such that human factors play a far less substantial role in image acquisition.

References

[1] A. Gefen, "Deep tissue injury from a bioengineering point of view." *Ostomy/wound management*, vol. 55, no. 4, pp. 26–36, Apr. 2009. [Online]. Available: http://view.ncbi.nlm.nih.gov/pubmed/19387094

[2] J. M. Black, L. E. Edsberg, M. M. Baharestani, D. Langemo, M. Goldberg, L. McNichol, J. Cuddigan, and National Pressure Ulcer Advisory Panel, "pressure ulcers: avoidable or unavoidable? results of the national pressure ulcer advisory panel consensus conference." *Ostomy/wound management*, vol. 57, no. 2, pp. 24–37, Feb. 2011. [Online]. Available: http://view.ncbi.nlm.nih.gov/pubmed/21350270

[3] R. M. Allman, P. S. Goode, M. M. Patrick, N. Burst, and A. A. Bartolucci, "Pressure ulcer risk factors among hospitalized patients with activity limitation." *JAMA : the journal of the American Medical Association*, vol. 273, no. 11, pp. 865–870, Mar. 1995. [Online]. Available: http://view.ncbi.nlm.nih.gov/pubmed/7869557

[4] C. A. Salzberg, D. W. Byrne, C. G. Cayten, P. van Niewerburgh, J. G. Murphy, and M. Viehbeck, "A new pressure ulcer risk assessment scale for individuals with spinal cord injury." *American journal of physical medicine & rehabilitation / Association of Academic*

Physiatrists, vol. 75, no. 2, pp. 96–104, 1996. [Online]. Available: http://view.ncbi.nlm.nih.gov/pubmed/8630201

[5] N. Kanno, T. Nakamura, M. Yamanaka, K. Kouda, T. Nakamura, and F. Tajima, "Low-echoic lesions underneath the skin in subjects with spinal-cord injury." *Spinal cord*, vol. 47, no. 3, pp. 225–229, Mar. 2009. [Online]. Available: http://dx.doi.org/10.1038/sc.2008.101

[6] J. Black, M. M. M. Baharestani, J. Cuddigan, B. Dorner, L. Edsberg, D. Langemo, M. E. E. Posthauer, C. Ratliff, G. Taler, and National Pressure Ulcer Advisory Panel, "National pressure ulcer advisory panel's updated pressure ulcer staging system." *Advances in skin & wound care*, vol. 20, no. 5, pp. 269–274, May 2007. [Online]. Available: http://dx.doi.org/10.1097/01.asw.0000269314.23015.e9

[7] C. V. Bouten, C. W. Oomens, F. P. Baaijens, and D. L. Bader, "The etiology of pressure ulcers: skin deep or muscle bound?" *Archives of physical medicine and rehabilitation*, vol. 84, no. 4, pp. 616–619, Apr. 2003. [Online]. Available: http://dx.doi.org/10.1053/apmr.2003.50038

[8] C. W. Oomens, S. Loerakker, and D. L. Bader, "The importance of internal strain as opposed to interface pressure in the prevention of pressure related deep tissue injury." *Journal of tissue viability*, vol. 19, no. 2, pp. 35–42, May 2010. [Online]. Available: http://dx.doi.org/10.1016/j.jtv.2009.11.002

[9] T. U. S. National Library of Medicine, "Visible human project," 1994.

[10] L. R. Solis, E. Twist, P. Seres, R. B. Thompson, and V. K. Mushahwar, "Prevention of deep tissue injury through muscle contractions induced by intermittent electrical stimulation after spinal

cord injury in pigs." *Journal of applied physiology (Bethesda, Md. : 1985)*, vol. 114, no. 2, pp. 286–296, Jan. 2013. [Online]. Available: http://dx.doi.org/10.1152/japplphysiol.00257.2012

[11] J. C. Bamber and R. J. Dickinson, "Ultrasonic b-scanning: a computer simulation." *Physics in medicine and biology*, vol. 25, no. 3, pp. 463–479, May 1980. [Online]. Available: http://view.ncbi.nlm.nih.gov/pubmed/7403261

[12] T. A. Krouskop, T. M. Wheeler, F. Kallel, B. S. Garra, and T. Hall, "Elastic moduli of breast and prostate tissues under compression," *Ultrasonic Imaging*, vol. 20, no. 4, pp. 260–274, Oct. 1998. [Online]. Available: http://dx.doi.org/10.1177/016173469802000403

[13] A. P. Choi and Y. P. Zheng, "Estimation of young's modulus and poisson's ratio of soft tissue from indentation using two different-sized indentors: finite element analysis of the finite deformation effect." *Medical & biological engineering & computing*, vol. 43, no. 2, pp. 258–264, Mar. 2005. [Online]. Available: http://view.ncbi.nlm.nih.gov/pubmed/15865137

[14] A. D. Martin, M. Z. Daniel, D. T. Drinkwater, and J. P. Clarys, "Adipose tissue density, estimated adipose lipid fraction and whole body adiposity in male cadavers." *International journal of obesity and related metabolic disorders : journal of the International Association for the Study of Obesity*, vol. 18, no. 2, pp. 79–83, Feb. 1994. [Online]. Available: http://view.ncbi.nlm.nih.gov/pubmed/8148928

[15] E. Brusseau, J. Kybic, J.-F. F. Deprez, and O. Basset, "2-D locally regularized tissue strain estimation from radio-frequency ultrasound images: theoretical developments and results on experimental data."

IEEE transactions on medical imaging, vol. 27, no. 2, pp. 145–160, Feb. 2008. [Online]. Available: http://dx.doi.org/10.1109/tmi.2007.897408

Chapter 4

Numerical Characterization of Acoustic Radiation Force Impulse Imaging

4.1 Introduction

Lorem ipsum dolor sit amet, consectetuer adipiscing elit. Ut purus elit, vestibulum ut, placerat ac, adipiscing vitae, felis. Curabitur dictum gravida mauris. Nam arcu libero, nonummy eget, consectetuer id, vulputate a, magna. Donec vehicula augue eu neque. Pellentesque habitant morbi tristique senectus et netus et malesuada fames ac turpis egestas. Mauris ut leo. Cras viverra metus rhoncus sem. Nulla et lectus vestibulum urna fringilla ultrices. Phasellus eu tellus sit amet tortor gravida placerat. Integer sapien est, iaculis in, pretium quis, viverra ac, nunc. Praesent eget sem vel leo ultrices bibendum. Aenean faucibus. Morbi dolor nulla, malesuada eu, pulvinar at, mollis ac, nulla. Curabitur auctor semper nulla. Donec varius orci eget risus. Duis nibh mi, congue eu, accumsan eleifend, sagittis quis, diam. Duis eget orci sit amet orci

dignissim rutrum.

4.2 Methods

Lorem ipsum dolor sit amet, consectetuer adipiscing elit. Ut purus elit, vestibulum ut, placerat ac, adipiscing vitae, felis. Curabitur dictum gravida mauris. Nam arcu libero, nonummy eget, consectetuer id, vulputate a, magna. Donec vehicula augue eu neque. Pellentesque habitant morbi tristique senectus et netus et malesuada fames ac turpis egestas. Mauris ut leo. Cras viverra metus rhoncus sem. Nulla et lectus vestibulum urna fringilla ultrices. Phasellus eu tellus sit amet tortor gravida placerat. Integer sapien est, iaculis in, pretium quis, viverra ac, nunc. Praesent eget sem vel leo ultrices bibendum. Aenean faucibus. Morbi dolor nulla, malesuada eu, pulvinar at, mollis ac, nulla. Curabitur auctor semper nulla. Donec varius orci eget risus. Duis nibh mi, congue eu, accumsan eleifend, sagittis quis, diam. Duis eget orci sit amet orci dignissim rutrum.

4.2.1 Numerical Model

Lorem ipsum dolor sit amet, consectetuer adipiscing elit. Ut purus elit, vestibulum ut, placerat ac, adipiscing vitae, felis. Curabitur dictum gravida mauris. Nam arcu libero, nonummy eget, consectetuer id, vulputate a, magna. Donec vehicula augue eu neque. Pellentesque habitant morbi tristique senectus et netus et malesuada fames ac turpis egestas. Mauris ut leo. Cras viverra metus rhoncus sem. Nulla et lectus vestibulum urna fringilla ultrices. Phasellus eu tellus sit amet tortor gravida placerat. Integer sapien est, iaculis in, pretium quis, viverra ac, nunc. Praesent eget sem vel leo ultrices bibendum. Aenean faucibus. Morbi dolor nulla, malesuada eu, pulvinar at, mollis ac, nulla.

Curabitur auctor semper nulla. Donec varius orci eget risus. Duis nibh mi, congue eu, accumsan eleifend, sagittis quis, diam. Duis eget orci sit amet orci dignissim rutrum.

Governing Equations

The governing equations use for this model were the set of coupled first-order partial differential equations 4.1. These equations are the first-order equivalents of 4.2 taking into account acoustic absorption, tissue heterogeneities, and acoustic wave non-linearities [**?**].

$$\nabla^2 p - \frac{1}{c_0^2}\frac{\partial^2 p}{\partial t^2} = 0 \tag{4.2}$$

Boundary and Initial Conditions

Lorem ipsum dolor sit amet, consectetuer adipiscing elit. Ut purus elit, vestibulum ut, placerat ac, adipiscing vitae, felis. Curabitur dictum gravida mauris. Nam arcu libero, nonummy eget, consectetuer id, vulputate a, magna. Donec vehicula augue eu neque. Pellentesque habitant morbi tristique senectus et netus et malesuada fames ac turpis egestas. Mauris ut leo. Cras viverra metus rhoncus sem. Nulla et lectus vestibulum urna fringilla ultrices. Phasellus eu tellus sit amet tortor gravida placerat. Integer sapien est, iaculis in, pretium quis, viverra ac, nunc. Praesent eget sem vel leo ultrices bibendum. Aenean faucibus. Morbi dolor nulla, malesuada eu, pulvinar at, mollis ac, nulla. Curabitur auctor semper nulla. Donec varius orci eget risus. Duis nibh mi, congue eu, accumsan eleifend, sagittis quis, diam. Duis eget orci sit amet orci dignissim rutrum.

4.3 Results

Lorem ipsum dolor sit amet, consectetuer adipiscing elit. Ut purus elit, vestibulum ut, placerat ac, adipiscing vitae, felis. Curabitur dictum gravida mauris. Nam arcu libero, nonummy eget, consectetuer id, vulputate a, magna. Donec vehicula augue eu neque. Pellentesque habitant morbi tristique senectus et netus et malesuada fames ac turpis egestas. Mauris ut leo. Cras viverra metus rhoncus sem. Nulla et lectus vestibulum urna fringilla ultrices. Phasellus eu tellus sit amet tortor gravida placerat. Integer sapien est, iaculis in, pretium quis, viverra ac, nunc. Praesent eget sem vel leo ultrices bibendum. Aenean faucibus. Morbi dolor nulla, malesuada eu, pulvinar at, mollis ac, nulla. Curabitur auctor semper nulla. Donec varius orci eget risus. Duis nibh mi, congue eu, accumsan eleifend, sagittis quis, diam. Duis eget orci sit amet orci dignissim rutrum.

Chapter 5

Numerical Characterization of Shear Wave Speed Quantification

Lorem ipsum dolor sit amet, consectetuer adipiscing elit. Ut purus elit, vestibulum ut, placerat ac, adipiscing vitae, felis. Curabitur dictum gravida mauris. Nam arcu libero, nonummy eget, consectetuer id, vulputate a, magna. Donec vehicula augue eu neque. Pellentesque habitant morbi tristique senectus et netus et malesuada fames ac turpis egestas. Mauris ut leo. Cras viverra metus rhoncus sem. Nulla et lectus vestibulum urna fringilla ultrices. Phasellus eu tellus sit amet tortor gravida placerat. Integer sapien est, iaculis in, pretium quis, viverra ac, nunc. Praesent eget sem vel leo ultrices bibendum. Aenean faucibus. Morbi dolor nulla, malesuada eu, pulvinar at, mollis ac, nulla. Curabitur auctor semper nulla. Donec varius orci eget risus. Duis nibh mi, congue eu, accumsan eleifend, sagittis quis, diam. Duis eget orci sit amet orci dignissim rutrum.

Chapter 6

Conclusion

Lorem ipsum dolor sit amet, consectetuer adipiscing elit. Ut purus elit, vestibulum ut, placerat ac, adipiscing vitae, felis. Curabitur dictum gravida mauris. Nam arcu libero, nonummy eget, consectetuer id, vulputate a, magna. Donec vehicula augue eu neque. Pellentesque habitant morbi tristique senectus et netus et malesuada fames ac turpis egestas. Mauris ut leo. Cras viverra metus rhoncus sem. Nulla et lectus vestibulum urna fringilla ultrices. Phasellus eu tellus sit amet tortor gravida placerat. Integer sapien est, iaculis in, pretium quis, viverra ac, nunc. Praesent eget sem vel leo ultrices bibendum. Aenean faucibus. Morbi dolor nulla, malesuada eu, pulvinar at, mollis ac, nulla. Curabitur auctor semper nulla. Donec varius orci eget risus. Duis nibh mi, congue eu, accumsan eleifend, sagittis quis, diam. Duis eget orci sit amet orci dignissim rutrum.

6.1 Clinical Need for DTI Detection

Lorem ipsum dolor sit amet, consectetuer adipiscing elit. Ut purus elit, vestibulum ut, placerat ac, adipiscing vitae, felis. Curabitur dictum gravida mauris. Nam arcu libero, nonummy eget, consectetuer id, vulputate a, magna. Donec

vehicula augue eu neque. Pellentesque habitant morbi tristique senectus et netus et malesuada fames ac turpis egestas. Mauris ut leo. Cras viverra metus rhoncus sem. Nulla et lectus vestibulum urna fringilla ultrices. Phasellus eu tellus sit amet tortor gravida placerat. Integer sapien est, iaculis in, pretium quis, viverra ac, nunc. Praesent eget sem vel leo ultrices bibendum. Aenean faucibus. Morbi dolor nulla, malesuada eu, pulvinar at, mollis ac, nulla. Curabitur auctor semper nulla. Donec varius orci eget risus. Duis nibh mi, congue eu, accumsan eleifend, sagittis quis, diam. Duis eget orci sit amet orci dignissim rutrum.

6.2 USE Provides Potential Diagnosis Capability

Lorem ipsum dolor sit amet, consectetuer adipiscing elit. Ut purus elit, vestibulum ut, placerat ac, adipiscing vitae, felis. Curabitur dictum gravida mauris. Nam arcu libero, nonummy eget, consectetuer id, vulputate a, magna. Donec vehicula augue eu neque. Pellentesque habitant morbi tristique senectus et netus et malesuada fames ac turpis egestas. Mauris ut leo. Cras viverra metus rhoncus sem. Nulla et lectus vestibulum urna fringilla ultrices. Phasellus eu tellus sit amet tortor gravida placerat. Integer sapien est, iaculis in, pretium quis, viverra ac, nunc. Praesent eget sem vel leo ultrices bibendum. Aenean faucibus. Morbi dolor nulla, malesuada eu, pulvinar at, mollis ac, nulla. Curabitur auctor semper nulla. Donec varius orci eget risus. Duis nibh mi, congue eu, accumsan eleifend, sagittis quis, diam. Duis eget orci sit amet orci dignissim rutrum.

6.3 Future Work

Lorem ipsum dolor sit amet, consectetuer adipiscing elit. Ut purus elit, vestibulum ut, placerat ac, adipiscing vitae, felis. Curabitur dictum gravida mauris. Nam arcu libero, nonummy eget, consectetuer id, vulputate a, magna. Donec vehicula augue eu neque. Pellentesque habitant morbi tristique senectus et netus et malesuada fames ac turpis egestas. Mauris ut leo. Cras viverra metus rhoncus sem. Nulla et lectus vestibulum urna fringilla ultrices. Phasellus eu tellus sit amet tortor gravida placerat. Integer sapien est, iaculis in, pretium quis, viverra ac, nunc. Praesent eget sem vel leo ultrices bibendum. Aenean faucibus. Morbi dolor nulla, malesuada eu, pulvinar at, mollis ac, nulla. Curabitur auctor semper nulla. Donec varius orci eget risus. Duis nibh mi, congue eu, accumsan eleifend, sagittis quis, diam. Duis eget orci sit amet orci dignissim rutrum.

6.3.1 Animal Studies?

Lorem ipsum dolor sit amet, consectetuer adipiscing elit. Ut purus elit, vestibulum ut, placerat ac, adipiscing vitae, felis. Curabitur dictum gravida mauris. Nam arcu libero, nonummy eget, consectetuer id, vulputate a, magna. Donec vehicula augue eu neque. Pellentesque habitant morbi tristique senectus et netus et malesuada fames ac turpis egestas. Mauris ut leo. Cras viverra metus rhoncus sem. Nulla et lectus vestibulum urna fringilla ultrices. Phasellus eu tellus sit amet tortor gravida placerat. Integer sapien est, iaculis in, pretium quis, viverra ac, nunc. Praesent eget sem vel leo ultrices bibendum. Aenean faucibus. Morbi dolor nulla, malesuada eu, pulvinar at, mollis ac, nulla. Curabitur auctor semper nulla. Donec varius orci eget risus. Duis nibh mi, congue eu, accumsan eleifend, sagittis quis, diam. Duis eget orci sit amet orci

dignissim rutrum.

6.3.2 Human Studies?

Lorem ipsum dolor sit amet, consectetuer adipiscing elit. Ut purus elit, vestibulum ut, placerat ac, adipiscing vitae, felis. Curabitur dictum gravida mauris. Nam arcu libero, nonummy eget, consectetuer id, vulputate a, magna. Donec vehicula augue eu neque. Pellentesque habitant morbi tristique senectus et netus et malesuada fames ac turpis egestas. Mauris ut leo. Cras viverra metus rhoncus sem. Nulla et lectus vestibulum urna fringilla ultrices. Phasellus eu tellus sit amet tortor gravida placerat. Integer sapien est, iaculis in, pretium quis, viverra ac, nunc. Praesent eget sem vel leo ultrices bibendum. Aenean faucibus. Morbi dolor nulla, malesuada eu, pulvinar at, mollis ac, nulla. Curabitur auctor semper nulla. Donec varius orci eget risus. Duis nibh mi, congue eu, accumsan eleifend, sagittis quis, diam. Duis eget orci sit amet orci dignissim rutrum.

References

[1] A. Gefen, "Deep tissue injury from a bioengineering point of view." *Ostomy/wound management*, vol. 55, no. 4, pp. 26–36, Apr. 2009. [Online]. Available: http://view.ncbi.nlm.nih.gov/pubmed/19387094

[2] J. M. Black, L. E. Edsberg, M. M. Baharestani, D. Langemo, M. Goldberg, L. McNichol, J. Cuddigan, and National Pressure Ulcer Advisory Panel, "pressure ulcers: avoidable or unavoidable? results of the national pressure ulcer advisory panel consensus conference." *Ostomy/wound management*, vol. 57, no. 2, pp. 24–37, Feb. 2011. [Online]. Available: http://view.ncbi.nlm.nih.gov/pubmed/21350270

[3] R. M. Allman, P. S. Goode, M. M. Patrick, N. Burst, and A. A. Bartolucci, "Pressure ulcer risk factors among hospitalized patients with activity limitation." *JAMA : the journal of the American Medical Association*, vol. 273, no. 11, pp. 865–870, Mar. 1995. [Online]. Available: http://view.ncbi.nlm.nih.gov/pubmed/7869557

[4] C. A. Salzberg, D. W. Byrne, C. G. Cayten, P. van Niewerburgh, J. G. Murphy, and M. Viehbeck, "A new pressure ulcer risk assessment scale for individuals with spinal cord injury." *American journal of physical medicine & rehabilitation / Association of Academic*

Physiatrists, vol. 75, no. 2, pp. 96–104, 1996. [Online]. Available: http://view.ncbi.nlm.nih.gov/pubmed/8630201

[5] N. Kanno, T. Nakamura, M. Yamanaka, K. Kouda, T. Nakamura, and F. Tajima, "Low-echoic lesions underneath the skin in subjects with spinal-cord injury." *Spinal cord*, vol. 47, no. 3, pp. 225–229, Mar. 2009. [Online]. Available: http://dx.doi.org/10.1038/sc.2008.101

[6] J. Black, M. M. M. Baharestani, J. Cuddigan, B. Dorner, L. Edsberg, D. Langemo, M. E. E. Posthauer, C. Ratliff, G. Taler, and National Pressure Ulcer Advisory Panel, "National pressure ulcer advisory panel's updated pressure ulcer staging system." *Advances in skin & wound care*, vol. 20, no. 5, pp. 269–274, May 2007. [Online]. Available: http://dx.doi.org/10.1097/01.asw.0000269314.23015.e9

[7] C. V. Bouten, C. W. Oomens, F. P. Baaijens, and D. L. Bader, "The etiology of pressure ulcers: skin deep or muscle bound?" *Archives of physical medicine and rehabilitation*, vol. 84, no. 4, pp. 616–619, Apr. 2003. [Online]. Available: http://dx.doi.org/10.1053/apmr.2003.50038

[8] C. W. Oomens, S. Loerakker, and D. L. Bader, "The importance of internal strain as opposed to interface pressure in the prevention of pressure related deep tissue injury." *Journal of tissue viability*, vol. 19, no. 2, pp. 35–42, May 2010. [Online]. Available: http://dx.doi.org/10.1016/j.jtv.2009.11.002

[9] T. U. S. National Library of Medicine, "Visible human project," 1994.

[10] L. R. Solis, E. Twist, P. Seres, R. B. Thompson, and V. K. Mushahwar, "Prevention of deep tissue injury through muscle contractions induced by intermittent electrical stimulation after spinal

cord injury in pigs." *Journal of applied physiology (Bethesda, Md. : 1985)*, vol. 114, no. 2, pp. 286–296, Jan. 2013. [Online]. Available: http://dx.doi.org/10.1152/japplphysiol.00257.2012

[11] J. C. Bamber and R. J. Dickinson, "Ultrasonic b-scanning: a computer simulation." *Physics in medicine and biology*, vol. 25, no. 3, pp. 463–479, May 1980. [Online]. Available: http://view.ncbi.nlm.nih.gov/pubmed/7403261

[12] T. A. Krouskop, T. M. Wheeler, F. Kallel, B. S. Garra, and T. Hall, "Elastic moduli of breast and prostate tissues under compression," *Ultrasonic Imaging*, vol. 20, no. 4, pp. 260–274, Oct. 1998. [Online]. Available: http://dx.doi.org/10.1177/016173469802000403

[13] A. P. Choi and Y. P. Zheng, "Estimation of young's modulus and poisson's ratio of soft tissue from indentation using two different-sized indentors: finite element analysis of the finite deformation effect." *Medical & biological engineering & computing*, vol. 43, no. 2, pp. 258–264, Mar. 2005. [Online]. Available: http://view.ncbi.nlm.nih.gov/pubmed/15865137

[14] A. D. Martin, M. Z. Daniel, D. T. Drinkwater, and J. P. Clarys, "Adipose tissue density, estimated adipose lipid fraction and whole body adiposity in male cadavers." *International journal of obesity and related metabolic disorders : journal of the International Association for the Study of Obesity*, vol. 18, no. 2, pp. 79–83, Feb. 1994. [Online]. Available: http://view.ncbi.nlm.nih.gov/pubmed/8148928

[15] E. Brusseau, J. Kybic, J.-F. F. Deprez, and O. Basset, "2-D locally regularized tissue strain estimation from radio-frequency ultrasound images: theoretical developments and results on experimental data."

IEEE transactions on medical imaging, vol. 27, no. 2, pp. 145–160, Feb. 2008. [Online]. Available: http://dx.doi.org/10.1109/tmi.2007.897408

Appendix A

Data Tables

Lorem ipsum dolor sit amet, consectetuer adipiscing elit. Ut purus elit, vestibulum ut, placerat ac, adipiscing vitae, felis. Curabitur dictum gravida mauris. Nam arcu libero, nonummy eget, consectetuer id, vulputate a, magna. Donec vehicula augue eu neque. Pellentesque habitant morbi tristique senectus et netus et malesuada fames ac turpis egestas. Mauris ut leo. Cras viverra metus rhoncus sem. Nulla et lectus vestibulum urna fringilla ultrices. Phasellus eu tellus sit amet tortor gravida placerat. Integer sapien est, iaculis in, pretium quis, viverra ac, nunc. Praesent eget sem vel leo ultrices bibendum. Aenean faucibus. Morbi dolor nulla, malesuada eu, pulvinar at, mollis ac, nulla. Curabitur auctor semper nulla. Donec varius orci eget risus. Duis nibh mi, congue eu, accumsan eleifend, sagittis quis, diam. Duis eget orci sit amet orci dignissim rutrum.

A.1 Quasi-Static Ultrasound Elastography

Lorem ipsum dolor sit amet, consectetuer adipiscing elit. Ut purus elit, vestibulum ut, placerat ac, adipiscing vitae, felis. Curabitur dictum gravida mauris. Nam arcu libero, nonummy eget, consectetuer id, vulputate a, magna. Donec

vehicula augue eu neque. Pellentesque habitant morbi tristique senectus et netus et malesuada fames ac turpis egestas. Mauris ut leo. Cras viverra metus rhoncus sem. Nulla et lectus vestibulum urna fringilla ultrices. Phasellus eu tellus sit amet tortor gravida placerat. Integer sapien est, iaculis in, pretium quis, viverra ac, nunc. Praesent eget sem vel leo ultrices bibendum. Aenean faucibus. Morbi dolor nulla, malesuada eu, pulvinar at, mollis ac, nulla. Curabitur auctor semper nulla. Donec varius orci eget risus. Duis nibh mi, congue eu, accumsan eleifend, sagittis quis, diam. Duis eget orci sit amet orci dignissim rutrum.

A.2 Acoustic Radiation Force Impulse Imaging

Lorem ipsum dolor sit amet, consectetuer adipiscing elit. Ut purus elit, vestibulum ut, placerat ac, adipiscing vitae, felis. Curabitur dictum gravida mauris. Nam arcu libero, nonummy eget, consectetuer id, vulputate a, magna. Donec vehicula augue eu neque. Pellentesque habitant morbi tristique senectus et netus et malesuada fames ac turpis egestas. Mauris ut leo. Cras viverra metus rhoncus sem. Nulla et lectus vestibulum urna fringilla ultrices. Phasellus eu tellus sit amet tortor gravida placerat. Integer sapien est, iaculis in, pretium quis, viverra ac, nunc. Praesent eget sem vel leo ultrices bibendum. Aenean faucibus. Morbi dolor nulla, malesuada eu, pulvinar at, mollis ac, nulla. Curabitur auctor semper nulla. Donec varius orci eget risus. Duis nibh mi, congue eu, accumsan eleifend, sagittis quis, diam. Duis eget orci sit amet orci dignissim rutrum.

A.3 Shear Wave Speed Quantification

Lorem ipsum dolor sit amet, consectetuer adipiscing elit. Ut purus elit, vestibulum ut, placerat ac, adipiscing vitae, felis. Curabitur dictum gravida mauris. Nam arcu libero, nonummy eget, consectetuer id, vulputate a, magna. Donec vehicula augue eu neque. Pellentesque habitant morbi tristique senectus et netus et malesuada fames ac turpis egestas. Mauris ut leo. Cras viverra metus rhoncus sem. Nulla et lectus vestibulum urna fringilla ultrices. Phasellus eu tellus sit amet tortor gravida placerat. Integer sapien est, iaculis in, pretium quis, viverra ac, nunc. Praesent eget sem vel leo ultrices bibendum. Aenean faucibus. Morbi dolor nulla, malesuada eu, pulvinar at, mollis ac, nulla. Curabitur auctor semper nulla. Donec varius orci eget risus. Duis nibh mi, congue eu, accumsan eleifend, sagittis quis, diam. Duis eget orci sit amet orci dignissim rutrum.

Appendix B

Source Code

Lorem ipsum dolor sit amet, consectetuer adipiscing elit. Ut purus elit, vestibulum ut, placerat ac, adipiscing vitae, felis. Curabitur dictum gravida mauris. Nam arcu libero, nonummy eget, consectetuer id, vulputate a, magna. Donec vehicula augue eu neque. Pellentesque habitant morbi tristique senectus et netus et malesuada fames ac turpis egestas. Mauris ut leo. Cras viverra metus rhoncus sem. Nulla et lectus vestibulum urna fringilla ultrices. Phasellus eu tellus sit amet tortor gravida placerat. Integer sapien est, iaculis in, pretium quis, viverra ac, nunc. Praesent eget sem vel leo ultrices bibendum. Aenean faucibus. Morbi dolor nulla, malesuada eu, pulvinar at, mollis ac, nulla. Curabitur auctor semper nulla. Donec varius orci eget risus. Duis nibh mi, congue eu, accumsan eleifend, sagittis quis, diam. Duis eget orci sit amet orci dignissim rutrum.

B.1 Quasi2DUltrasound

Lorem ipsum dolor sit amet, consectetuer adipiscing elit. Ut purus elit, vestibulum ut, placerat ac, adipiscing vitae, felis. Curabitur dictum gravida mauris. Nam arcu libero, nonummy eget, consectetuer id, vulputate a, magna. Donec

vehicula augue eu neque. Pellentesque habitant morbi tristique senectus et netus et malesuada fames ac turpis egestas. Mauris ut leo. Cras viverra metus rhoncus sem. Nulla et lectus vestibulum urna fringilla ultrices. Phasellus eu tellus sit amet tortor gravida placerat. Integer sapien est, iaculis in, pretium quis, viverra ac, nunc. Praesent eget sem vel leo ultrices bibendum. Aenean faucibus. Morbi dolor nulla, malesuada eu, pulvinar at, mollis ac, nulla. Curabitur auctor semper nulla. Donec varius orci eget risus. Duis nibh mi, congue eu, accumsan eleifend, sagittis quis, diam. Duis eget orci sit amet orci dignissim rutrum.